PhD thesis

Jagiellonian University in Kraków
Department of Physics, Astronomy
and Applied Computer Science.

Quantum phase transitions

Author:
Marek M. Rams

Supervisor: dr hab. Jacek Dziarmaga

Reviewers: prof. dr hab. Jakub Zakrzewski
dr hab. Piotr Tomczak

For my Parents

Acknowledgment

Foremost, I would like to express my sincere gratitude to my supervisor Jacek Dziarmaga. His enthusiasm, wide knowledge and continuous support helped me in all the time of my research and writing of this thesis. I could not have imagined having a better advisor and mentor.

I owe my deepest gratitude to Bogdan Damski and Michael Zwolak for offering me long-term graduate research assistant position at Los Alamos National Laboratory and possibility to work with them on exciting projects. Their influence on my development as a physicist is extraordinary.

I would like to thank many researchers I was lucky to meet at my path and interact with, especially Lukasz Cincio, Maciej Lewenstein, Armand Niederberger and Wojciech Zurek.

The preparing of this thesis was supported by doctoral dissertation grant awarded by the Ministry of Science and Higher Education, grant number N202 174335.

Last but not the least, I would like to thank my family for constant support and encouragement and in particularly my older brother Michal for a lot of invaluable advices.

Contents

Chapter 1

Introduction

The possibility of having phase transition at very low – in particular zero – temperature which origins are purely quantum was first put forward by John Hertz in 1976 [1]. Initially it was rather theoretical curiosity but due to the later experimental development subsequently it became a field of intense research. Such transition i.e. Quantum Phase Transitions, although in many respects similar, are fundamentally different than their classical counterpart [2]. For instance, the fluctuation which are driving the transition are purely quantum and not thermal – which is the case for the classical transition where quantum origins of underlying physics are suppressed by finite temperature.

The experiments demonstrating quantum phase transition include [3, 4] where the transition from superfluid to Mott insulator in ultracold atomic gases confined in an optical lattice was observed. Other prominent examples count spin magnetic systems like Ising chain [5] or spin-1 Bose-Einstein condensate [6]. It is also believed that quantum phase transition may play an important role in describing high-T_c superconductors when the dopant concentration is changed [7].

In this thesis I will address the important topic of quench dynamics through quantum critical points.

The general theory describing what is happening when we cross the critical point at a finite rate is given by Kibble-Zurek mechanism and was first put forward in the context of finite temperature transition. It was originally proposed by Kibble in the cosmological context [8]. Kibble studied spontaneously broken gauge theory to describe the early Universe. He argues that during a cooling of the early Universe and possible phase transition from 'normal' phase to the broken symmetry phase a structure of domain walls, strings or monopoles should arise.

Later the theory was extended to general condensed matter systems by Zurek [9]. He used the universal concepts of healing length and relaxation time (singular at the critical point) to predict how the number of topological defects after the transition through the critical point depends on transition rate and universality class.

Kibble-Zurek mechanism at finite temperature was extensively studied. Among others, it was confirmed numerically for the kinks formation during nonequilibrium relaxation of time-dependent Ginzburg-Landau model in 1D [10] and vortex formation during the quench of 2D superconductor described by complex scalar field minimally coupled to electromagnetism – i.e. the Abelian-Higgs model [11].

Besides, it was tested in great body of experiments including nematic liquid crystal

[12, 13], neutron-irradiated superfluid ^{3}He [14, 15], both high-T_c [16] and low-T_c superconductors [17], nonlinear optical system [18, 19] and vortex formation during Bose-Einstein condensation driven by evaporative cooling [20]. Those experimental results are consistent with Kibble-Zurek Mechanism, although more work is definitely needed to allow for more rigorous experimental tests of the theory.

Still, the zero temperature limit – related to Quantum Phase Transitions – is qualitatively different from finite temperature one outlined above. Indeed, the time evolution of a quantum system is unitary, so there is no damping and there are no thermal fluctuations that could initiate symmetry breaking in Kibble-Zurek mechanism. The final quantum state is not a single broken symmetry configuration but may – and in principle will - be in a superposition of all the possible configurations. The recent progress on quench dynamics of quantum phase transitions is mostly theoretical. It was initiated by works [21, 22] where – among others – the authors extended general, universal prediction based on Kibble-Zurek mechanism to quantum critical systems. Substantial amount of work has been put lately to better understand the nonequalibrium dynamics close to quantum critical points and subsequent relaxation of (excited) state. This can be seen in two very recent review articles [23, 24] and numerous references therein. One experimental example is provided by an instantaneous quench from paramagnetic to ferromagnetic phase in a dipolar Bose-Einstein condensate [6]. The formation of mosaic of finite-size ferromagnetic domains was observed there but, since the transition was effectively instantaneous, the relation between Kibble-Zurek scaling and transition rate could not have been checked.

The recent motivation for studying quench dynamics in quantum critical systems is mainly twofold. On the one hand, it originates from the idea of quantum simulators - see e.g. [25, 26] – which can be tracked back to Feynman and is closely related to adiabatic quantum computation. Lets say that a solution of some computational problem can be encoded into a ground state of a Hamiltonian $H_{\mathcal{F}}$ (adiabatic quantum computation). Equivalently we may be simply interested in the properties of the ground state of $H_{\mathcal{F}}$ (quantum simulators). The ground state itself, however, is extremely hard to prepare. The idea to circumvent that problem is to prepare a ground state for some Hamiltonian $H_{\mathcal{I}}$ for which it is easy to do so. Subsequently, we slowly and smoothly transform $H_{\mathcal{I}}$ into $H_{\mathcal{F}}$ in such a way that the state of the system follows adiabatically instantaneous ground state of changing Hamiltonian. We want to end up with desired ground state of $H_{\mathcal{F}}$. Moreover, as shown in [27] every quantum algorithm can be reformulated in such a way. Possibility of such an approach is limited by the fact that for specific instant of time we might expect vanishing energy gap of instantaneous Hamiltonian. This, in principle, leads to exciting the system as described by Kibble-Zurek mechanism. Here, it is, in a sense, a negative result and we look for condition under which we are able to cross the critical point in the adiabatic manner.

On the other hand motivation steams from the recent technological development in controlling ultra-cold atomic gases confined in optical lattices [28]. It is possible to control – to the unprecedented degree – parameters of the Hamiltonian. What is more they can be precisely change in time providing a feasible test bed for studying dynamical processes.

In this thesis I will focus mostly – but not only – on studying quench dynamics in quantum Ising model. This is the prototypical, not trivial model of quantum phase transition [2]. While, or maybe because, it is rather simply it allows us for detailed physical understanding of basic processes governing quench dynamics. The model, in many cases,

is exactly solvable and even if analytical results cannot be obtained it allows for quite precise and easily interpreted numerical results. It makes it a model of choice when we want to unravel the underlying physics which then can be used to better understand systems that are more complicated and considerably harder to analyze.

The thesis is organized as follow:

In Chapter 2 we will introduced Kibble-Zurek mechanism in more details and study quench dynamics in homogenous systems. We will focus on properties of the state of the system during and after the transition. We will be able to differentiate universal behavior resulting from Kibble-Zurek mechanism from non-universal processes connected with dephasing of the (excited) state after the transition. In order to do so we will discuss correlation function and fidelity between the ground state of the system and excited finite state after the evolution.

In Chapter 3 we will establish the theorem extending standard Kibble-Zurek mechanism to quenches that are additionally inhomogeneous in space. We will distinguish between non-adiabatic (Kibble-Zurek like) regime and adiabatic regime of the transition. The later provides a natural way to effectively 'avoid' critical point in order to cross it without exciting the system.

In Chapter 4 we will focus on dynamics in open systems. We will discuss specific example of the Ising model coupled to local spin environment. In our example the decoherence, which is caused by interaction with environment, has a profound effects on quench dynamics making it exponentially harder to cross the critical point in an adiabatic way.

While the results below are established for the one-dimensional quantum Ising and XY models, we conjecture that similar behavior should be encountered in other quantum phase transitions, and that their non-equilibrium evolution can be anticipated using equilibrium critical exponents and Kibble-Zurek mechanism.

Chapter 2

Homogeneus quench

In this chapter we will discuss the state of the system after slow dynamical transition across quantum critical point. We will start with more detailed discussion of Kibble-Zurek argument for quantum system [22]. Then we will proceed with analytical solution of the problem for the Ising model shown for the first time in [29]. We will calculate various quantities describing the – exited – final state. In adition to the 'classical' density of excitations we will use several other measures giving good characterization of the state. We will discuss in details the correlation functions and quantum fidelity between the final state of the system and the ground state. This chapter broadly extends the results published in [I].

To set the scene and to gain a better intuition we will start by introducing quantum Ising model. According to Sachdev [2], the understanding of quantum phase transitions is based on two prototypical models. One is the quantum rotor model and the other is – just mentioned – one-dimensional quantum Ising model. Of the two only the Ising model is exactly solvable. It is defined by the Hamiltonian:

$$H \;=\; -\sum_{n=1}^{N}\left(\sigma_n^x\sigma_{n+1}^x + g\sigma_n^z\right)\;. \tag{2.1}$$

where we assume periodic boundary conditions

$$\vec{\sigma}_{N+1} \;=\; \vec{\sigma}_1\;.$$

Quantum phase transition takes place at the critical value of the external magnetic field $g_c = \pm 1$. When $|g| > 1$, the ground state of the system is a paramagnet. In particular, when $g \gg 1$ all spins are polarized along the z-axis pointing in the direction of the magnetic field i.e. $|\ldots \uparrow\uparrow\uparrow\uparrow\uparrow\uparrow\uparrow\uparrow\uparrow\uparrow\uparrow\uparrow \ldots\rangle$. On the other hand, when $|g| < 1$ we have doubly degenerated ferromagnetic ground states (in the limit of infinite system size i.e. $N \to \infty$) with nonzero mean value of the order parameter $\langle\sigma_x\rangle$. In particular, when $g = 0$ all the spins are pointing either up or down along the x-axis. i.e. $|\ldots \rightarrow\rightarrow\rightarrow\rightarrow\rightarrow\rightarrow\rightarrow\rightarrow\rightarrow\rightarrow\rightarrow\rightarrow \ldots\rangle$ or $|\ldots \leftarrow\leftarrow\leftarrow\leftarrow\leftarrow\leftarrow\leftarrow\leftarrow\leftarrow\leftarrow\leftarrow\leftarrow \ldots\rangle$. The critical point is characterized by universal critical exponents. Among others – in typical cases for continuous transition – correlation length ξ is divergent near the critical point as $|g-g_c|^{-\nu}$ and excitation gap Δ vanishes at the critical point like $|g-g_c|^{z\nu}$. This defines critical exponents ν and z. For the Ising model we have $z = \nu = 1$. The standard (static)

solution of the Ising model and derivation of the critical exponents is shown in Appendix A.

2.1 Kibble-Zurek mechanism

In an infinitesimally slow classical transition from paramagnet to ferromagnet, the system would choose one of the two ferromagnetic states. In the analogous quantum case, any superposition of these two states is also a 'legal' ground state providing it is consistent with other quantum numbers (e.g. parity as is the case in the Ising model) conserved by the transition from the initial paramagnetic state.

However, when the size of the system $N \to \infty$, then the energy gap Δ at the critical point g_c tends to zero and it is impossible to pass the critical point at a finite speed without exciting the system. As a result, the system ends in a quantum superposition of states like:

$$|\cdots\rightarrow\leftarrow\leftarrow\leftarrow\leftarrow\leftarrow\leftarrow\rightarrow\rightarrow\rightarrow\rightarrow\rightarrow\rightarrow\leftarrow\leftarrow\leftarrow\leftarrow\leftarrow\leftarrow\rightarrow\rightarrow\rightarrow\rightarrow\rightarrow\rightarrow\leftarrow\ldots\rangle$$

with finite domains of spins pointing up or down (along x-axis in the Ising model (2.1)) and separated by kinks where the polarization of spins changes its orientation. Average size of the domains or, equivalently, average density of kinks depends on a transition rate. When the transition is slow, then the domain size is large, but when it is very fast, then orientation of individual spins can become random, uncorrelated with their nearest neighbors.

It is convenient to introduce here a dimensionless parameter $\epsilon = \frac{g-g_c}{g_c}$ which measures the distance from the critical point. Transition time τ_Q can be unambiguously defined when we assume that close to the critical point at $\epsilon = 0$ time-dependent field $\epsilon(t)$ driving the transition can be approximated by a linear quench

$$\epsilon(t) \;=\; -\frac{t}{\tau_Q} \tag{2.2}$$

with the adjustable quench rate τ_Q. We start the quench in 'normal' phase when $\epsilon \gg 0$ and end the transition well in broken symmetry phase with $\epsilon \ll 0$.

One can assume the adiabatic-impulse approximation [30, 31]. The quench begins in the ground state at large initial ϵ and the initial part of the evolution is adiabatic: the state follows the instantaneous ground state of the system. The evolution becomes non-adiabatic close to the critical point when the 'reaction time' of the quantum system given by the invers of the energy gap is comparable with the timescale at which the Hamiltonian is changing:

$$\frac{1}{gap[\epsilon(t)]} \;\sim\; \frac{gap[\epsilon(t)]}{|\frac{d}{dt}gap[\epsilon(t)]|} \tag{2.3}$$

This condition leads to an equation solved by

$$\hat{t} \sim \tau_Q^{\frac{z\nu}{z\nu+1}} \tag{2.4}$$

which gives the instant when the adiabatic to impulse transition occurs. This is equivalent to

$$\hat{\epsilon} \sim \tau_Q^{\frac{-1}{z\nu+1}} \tag{2.5}$$

which corresponds to the coherence length in the ground state:

$$\hat{\xi} \;=\; \tau_Q^{\frac{\nu}{z\nu+1}} \;. \tag{2.6}$$

Assuming impulse approximation, the quantum state does not change during the following non-adiabatic stage of the evolution between $\hat{\epsilon}$ and $-\hat{\epsilon}$ when the relaxation time is in principle much larger then the time at which the Hamiltonian is changing. Consequently, the quantum state at $-\hat{\epsilon}$ is expected to be approximately the ground state at $\hat{\epsilon}$ with the coherence length proportional to $\hat{\xi}$ and this is the initial state for the final adiabatic stage of the evolution after $\hat{\epsilon}$. This argument shows that when passing across the critical point, the state of the system gets imprinted with a finite Kibble-Zurek correlation length proportional to $\hat{\xi}$. In particular, this coherence length determines average density of kinks d after the transition

$$d \;\sim\; \frac{1}{\hat{\xi}} \;\sim\; \frac{1}{\tau_Q^{\frac{\nu}{1+z\nu}}} \;. \tag{2.7}$$

In particularly in the Ising model we predict

$$d \;\sim\; \frac{1}{\tau_Q^{1/2}} \;. \tag{2.8}$$

This is an order of magnitude estimate with an unknown $\mathcal{O}(1)$ prefactor. The estimate – and presented above line of rezoning – was first verified by numerical simulations in Ref. [22] and not much later the problem was solved exactly in Ref. [29], see also Ref. [32].

Note that when τ_Q is large enough, then $\hat{\epsilon}$ is small and the linearization in Eq. (2.2) is self-consistent: the Kibble-Zurek mechanism physics happens very close to the critical point between $-\hat{\epsilon}$ and $+\hat{\epsilon}$ and in principle we can expect that it is universal.

As we will see that general argument and adiabatic-impulse-adiabatic approximation allows us to predict the behavior of many other quantities describing the final state after evolution. However there are other – non-universal – effects related with subsequent evolution of the excited state which also have to be taken into account.

2.2 Ising model: dynamic solution and simply results

We check the above predictions by looking at the Ising model (2.1). The magnetic field is ramped down like

$$g(t<0) \;=\; -\frac{t}{\tau_Q} \tag{2.9}$$

coming from paramagnetic $g \gg 1$ at $t_{init} = -\infty$ to ferromagnetic $g = 0$ at $t_{final} = 0$.

In order to solve the dynamical problem we proceed similarly as in the static case (Appendix A) following [29, I]. After the Jordan-Wigner transformation (A.3) to fermionic creation-anihilation operators and subsequent Fourier transform the Hamiltonian takes the form (see A.9):

$$H^+ \;= \sum_k \left\{ 2[g-\cos(k)]c_k^\dagger c_k + \sin(k)\left[c_k^\dagger c_{-k}^\dagger + c_{-k}c_k\right] - g \right\} \;. \tag{2.10}$$

Since the initial state of the system (the ground state with large external magnetic field) has even number of quasiparticles, and the Hamiltonian conserve parity so we can restrict ourselves to H^+ with 'half-integer' momenta $k = \pm\frac{\pi}{2N}, \frac{3\pi}{2N}, \ldots, \frac{(2N-1)\pi}{2N}$, see (A.8).

The initial ground state is Bogoliubov vacuum $|0\rangle$ annihilated by all quasiparticle operators γ_k (A.10) which are determined by the asymptotic form of the (positive energy) Bogoliubov modes $(u_k, v_k) \simeq (1, 0)$ in the regime of $g \gg 1$.

When $g(t)$ is ramped down, the quantum state $|\psi(t)\rangle$ gets excited from the instantaneous ground state. We use time-dependent Bogoliubov method which makes an Ansatz that $|\psi(t)\rangle$ is a Bogoliubov vacuum annihilated by a set of quasiparticle annihilation operators $\tilde{\gamma}_k$ defined by a time-dependent Bogoliubov transformation

$$\begin{aligned} c_k &= u_k(t)\tilde{\gamma}_k + v^*_{-k}(t)\tilde{\gamma}^\dagger_{-k} \ , \\ c^\dagger_k &= u_k(t)^*\tilde{\gamma}^\dagger_k + v_{-k}(t)\tilde{\gamma}_{-k} \ , \end{aligned} \tag{2.11}$$

with the initial condition $[u_k(-\infty), v_k(-\infty)] = (1, 0)$ when $g \gg 1$.

In the Heisenberg picture, the Bogoliubov modes $[u_k(t), v_k(t)]$ must satisfy Heisenberg equation $i\frac{d}{dt}c_k = [c_k, H^+]$ with the constraint that $\frac{d}{dt}\tilde{\gamma}_k = 0$. The Heisenberg equation is equivalent to the dynamical version of the Bogoliubov-de Gennes equations (A.11):

$$\begin{aligned} i\frac{d}{dt}u_k &= +2\left[g(t) - \cos k\right] u_k + 2\sin k \ v_k \ , \\ i\frac{d}{dt}v_k &= -2\left[g(t) - \cos k\right] v_k + 2\sin k \ u_k \end{aligned} \tag{2.12}$$

We use the units such that $\hbar = 1$ and lattice spacing $a = 1$.

At any value of g, eqs. (2.12) have two instantaneous eigenstates. Initially, the mode $[u_k(t), v_k(t)]$ is the positive energy eigenstate (corresponding to the ground state), but during the quench it gets "excited" to a combination of the positive and negative (static) modes (A.13,A.16). At the end of the quench at $t_{final} = 0$ when $g = 0$ we have

$$[u_k(0), v_k(0)] = A_k\left(u_k, v_k\right) + B_k\left(u^-_k, v^-_k\right) \tag{2.13}$$

and consequently $\tilde{\gamma}_k = A_k\gamma_k - B_k\gamma^\dagger_k$, where γ_k annihilates static ground state at the final g (A.15). The final state which is, by construction, annihilated by both $\tilde{\gamma}_k$ and $\tilde{\gamma}_{-k}$ is

$$|\psi(0)\rangle = \prod_{k>0}\left(A_k + B_k\gamma^\dagger_k\gamma^\dagger_{-k}\right)|g = 0\rangle \ . \tag{2.14}$$

Pairs of quasiparticles with pseudomomenta $(k, -k)$ are excited together with probability

$$p_k = |B_k|^2 \ , \tag{2.15}$$

This probability can be found by mapping Eqs. (2.12) to the Landau-Zener (LZ) problem. Close similarity between Kibble-Zurek mechanism and Landau-Zenner problem was first pointed out in Ref. [30].

In order to do it we use transformation

$$\tau = 4\tau_Q \sin k\left(-\frac{t}{\tau_Q} + \cos k\right) \tag{2.16}$$

which brings Eqs. (2.12) to the standard Landau-Zener form [33]:

$$\begin{aligned} i\frac{d}{d\tau}u_k &= -\frac{1}{2}(\tau\Delta_k)u_k + \frac{1}{2}v_k \ , \\ i\frac{d}{d\tau}v_k &= +\frac{1}{2}(\tau\Delta_k)v_k + \frac{1}{2}u_k \ . \end{aligned} \tag{2.17}$$

with $\Delta_k^{-1} = 4\tau_Q \sin^2 k$. Here the time τ runs from $-\infty$ to $\tau_{\rm final} = 2\tau_Q \sin(2k)$ corresponding to $t_{final} = 0$. Tunneling between the positive and negative energy eigenstates happens when $\tau \in (-\Delta_k^{-1}, \Delta_k^{-1})$. $\tau_{\rm final}$ is well outside this interval, i.e. $\tau_{\rm final} \gg \Delta_k^{-1}$, for long wavelength modes with $|k| \ll 1$. For these modes, time τ in Eqs. (2.17) can be extended to $+\infty$ making them fully equivalent to LZ equations [33]. This equivalence can be used to easily obtain several simple results described below.

In the limit of slow transitions we can assume that only long wavelength modes, which have small gaps at their anti-crossing points, can get excited. For these modes, we can use the Landau-Zenner formula [33] for excitation probability:

$$p_k \ \simeq \ e^{-\frac{\pi}{2\Delta_k}} \ \simeq \ e^{-2\pi\tau_Q k^2} \ . \tag{2.18}$$

This approximation is self-consistent only when the width of the obtained Gaussian function $(4\pi\tau_Q)^{-1/2}$ is much less than 1 or, equivalently, for slow enough quenches with $\tau_Q \gg 1$. With the Landau-Zenner formula (2.18), we can easily calculate the number of kinks at final $g = 0$.

$$\mathcal{N} \ = \ \frac{1}{2}\langle\psi(0)|\sum_n \left(1 - \sigma_n^x\sigma_{n+1}^x\right)|\psi(0)\rangle \ = \ \langle\psi(0)|\sum_k \gamma_k^\dagger\gamma_k|\psi(0)\rangle. \tag{2.19}$$

(see Appendix A and note that g=0 here which simplifies the expression for $\sigma_n^x\sigma_{n+1}^x$). Since the probability of excitation

$$p_k = \langle\psi(0)|\gamma_k^\dagger\gamma_k|\psi(0)\rangle$$

we get

$$\mathcal{N} \ = \ \sum_k \ p_k \ . \tag{2.20}$$

There are at least two interesting cases:

Firstly, when $N \to \infty$ the sum in Eq. (2.20) can be replaced by an integral. The expectation value of density of kinks becomes

$$d = \lim_{N\to\infty}\frac{\mathcal{N}}{N} = \frac{1}{2\pi}\int_{-\pi}^{\pi} dk \ p_k = \frac{1}{2\pi}\frac{1}{\sqrt{2\tau_Q}}. \tag{2.21}$$

The density scales like $\tau_Q^{-1/2}$ in agreement with Kibble-Zurek mechanism, see Eq. (2.8). As expected, the slower quenches lead to fewer defects.

Secondly, we can ask what the fastest τ_Q is when no kinks get excited in a finite chain of size N. This critical τ_Q marks a crossover between adiabatic and non-adiabatic regimes. In other words, we can ask what is the probability for a finite chain to stay in

the ground state. As different pairs of quasiparticles $(k,-k)$ evolve independently, the probability to stay in the ground state is the product

$$\mathcal{P}_{\rm GS} \;=\; \prod_{k>0}(1-p_k)\;. \tag{2.22}$$

Well on the adiabatic side only the pair with lowest momentum $k=\pm\frac{\pi}{N}$ is likely to get excited and we can approximate

$$\mathcal{P}_{\rm GS} \;\approx\; 1-p_{\frac{\pi}{N}} \;\approx\; 1-\exp\left(-2\pi^3\frac{\tau_Q}{N^2}\right)\;. \tag{2.23}$$

A quench in a finite chain is adiabatic when

$$\tau_Q \;\gg\; \frac{N^2}{2\pi^3}\;. \tag{2.24}$$

Reading this inequality from right to left, the size N of a defect-free chain grows like $\tau_Q^{1/2}$ which is consistent with Eq. (2.8,2.21). Other way of looking at the same problem is through Finite Size Scaling. Finite size effects effectively round off the critical point which results in the finite gap at the critical point $\Delta\sim N^{-z}$ and maximum correlation length at the critical point is truncated by the size of the system $\xi=N$ (we work here in one spatial dimension – extension to $d>1$ is trivial). We can easily see that equation (2.3) cannot be satisfied when $N\ll\hat{\xi}$ and we stay in the adiabatic regime during the whole evolution – still with the possibility of exponentially small, noncollective excitations.

The full solution of the Landau-Zener equation (2.17) is given in general by Weber functions and is presented in Appendix B. In the interesting case of slow quenches ($\tau_Q\gg 1$) the modes after the transition for finite g=0 can be approximated as:

$$\begin{aligned}
|u_k|^2 &= \frac{1-\cos k}{2}+e^{-2\pi\tau_Q k^2}\;,\\
|v_k|^2 &= 1-|u_k|^2\;,\\
u_k v_k^* &= \frac{1}{2}\sin k+\mathrm{sign}(k)\;e^{-\pi\tau_Q k^2}\sqrt{1-e^{-2\pi\tau_Q k^2}}\;e^{i\varphi_k}\;,\\
\varphi_k &= \frac{\pi}{4}+2\tau_Q-(2-\ln 4)\tau_Q k^2+k^2\tau_Q\ln\tau_Q-\arg\left[\Gamma\left(1+i\tau_Q k^2\right)\right]\;.
\end{aligned} \tag{2.25}$$

(for comparison the static modes are $|u_k^{g=0}|^2=\frac{1-\cos k}{2}$ and $u_k^{g=0}v_k^{g=0}=\frac{1}{2}\sin k$). These products depend on k and τ_Q through two combinations: $\tau_Q k^2$, which implies the usual Kibble-Zurek mechanism coherence length $\hat{\xi}=\sqrt{\tau_Q}$, and $k^2\tau_Q\ln\tau_Q$. This will imply a second length scale $l=\sqrt{\tau_Q}\ln\tau_Q$ (see the following section). The final quantum state at $g=0$ cannot be characterized by a single scale of length. Physically, this appears to reflect a combination of two processes: Kibble-Zurek mechanism that sets up initial post-transition state of the system, and the subsequent evolution that can be regarded as quantum phase ordering. We will discuss this in greater details in the following sections.

We note here that the used approximation in (2.25) breaks unitarity of modes (u_k,v_k) and whenever it is relevant for the calculations we have to impose it by hand.

2.3 Correlation functions

Two-point correlation functions are of fundamental interest in phase transitions because they provide direct manifestation of their universal properties and are in general accessible experimentally for example via neutron scattering [2]. In this paragraph I will present results for spin-spin correlation functions during and after a quench across quantum phase transition.

To begin with, we observe that for symmetry reasons the ferromagnetic magnetization $\langle \sigma^x \rangle = 0$ throughout the quench. The transverse magnetization after the quench, however, is nonzero and reads:

$$\langle \psi(0)|\sigma_n^z|\psi(0)\rangle \;=\; \langle 1 - 2c_n^\dagger c_n \rangle \;=\; 2\alpha_0 - 1 \;\approx\; \frac{1}{2\pi\sqrt{2\tau_Q}}\;, \tag{2.26}$$

which is valid when $\tau_Q \gg 1$. This is what remains of the initial magnetization $\langle \sigma_n^z \rangle = 1$ in the initial ground state at $g \to \infty$. As expected, when the linear quench is slow, then the final magnetization decays towards $\langle \sigma_n^z \rangle = 0$ attributed to the ground state at the final $g = 0$.

We define here:

$$\begin{aligned} \alpha_{m-n} &= \alpha_{m,n} = \langle c_m c_n^\dagger \rangle \\ \beta_{m-n} &= \beta_{m,n} = \langle c_m c_n \rangle \end{aligned} \tag{2.27}$$

where state for which we calculate the avarange will depend on the context.

2.3.1 Correlations after the quench

In case of the state after the transition for $g = 0$ the avaranges in Eq. (2.27) can be calculated from approximated expressions (2.25)

$$\alpha_{m-n} = \frac{1}{2\pi}\int_{-\pi}^{\pi} dk\; |u_k|^2\; e^{ik(m-n)} \;\overset{\tau_Q \gg 1}{\approx}\; \frac{1}{2}\delta_{0,|m-n|} - \frac{1}{4}\delta_{1,|m-n|} + \frac{e^{-\frac{(m-n)^2}{8\pi\;\hat{\xi}^2}}}{2\sqrt{2}\pi\;\hat{\xi}}\;. \tag{2.28}$$

We note that α_{m-n} depends only on Kibble-Zurek dynamical correlation length $\hat{\xi}$. On the other hand,

$$\begin{aligned} \beta_{m-n} \;&=\; \frac{1}{2\pi i}\int_{-\pi}^{\pi} dk\; u_k v_k^*\; e^{ik(m-n)} \;\overset{\ln\tau_Q \gg 1}{\approx} \\ &\text{sign}(m-n)\;\left[\frac{1}{4}\delta_{1,|m-n|} - \frac{e^{i\left(2\tau_Q - \frac{|m-n|^2}{4\;\hat{\xi} l}\right)}}{2\sqrt{\pi\;\hat{\xi}\;l}} e^{-\frac{\pi|m-n|^2}{4\;l^2}}\sqrt{1 - e^{-\frac{\pi|m-n|^2}{2\;l^2}}}\right] \end{aligned} \tag{2.29}$$

which depends on both $\hat{\xi}$ and

$$l \;=\; \sqrt{\tau_Q}\ln\tau_Q\;. \tag{2.30}$$

We proceed with calculation of final transverse spin-spin correlation function at $g = 0$:

$$C_R^{zz} \equiv \langle \sigma_n^z \sigma_{n+R}^z \rangle - \langle \sigma_n^z \rangle \langle \sigma_{n+R}^z \rangle = 4\left(|\beta_R|^2 - |\alpha_R|^2\right) \approx \frac{e^{-\frac{\pi R^2}{2\, l^2}}\left(1 - e^{-\frac{\pi R^2}{2\, l^2}}\right)}{\pi\, \hat{\xi}\, l} - \frac{e^{-\frac{R^2}{\pi\, \hat{\xi}^2}}}{2\pi^2\, \hat{\xi}^2}\,, \tag{2.31}$$

when $R > 1$ and $\ln \tau_Q \gg 1$. This correlation function depends on both $\hat{\xi}$ and l. Long range correlations

$$C_R^{zz} \sim e^{-\frac{\pi R^2}{2\, l^2}} \tag{2.32}$$

decay in a Gaussian way on the scale l.

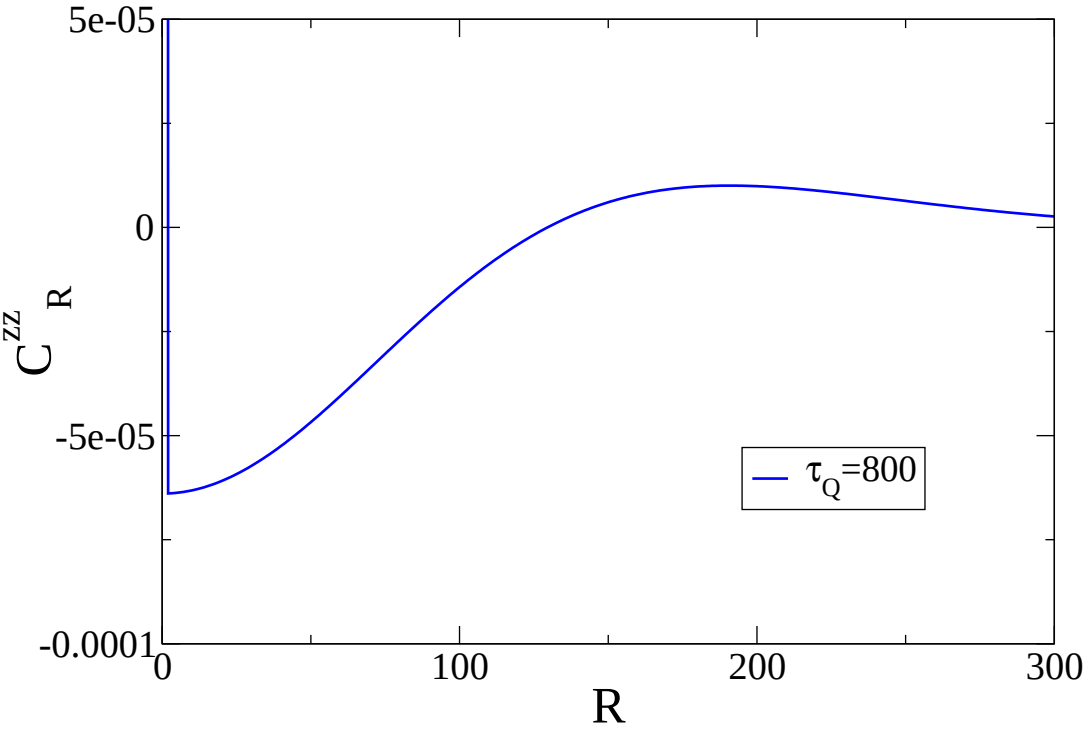

Figure 2.1: Correlation function C_R^{zz} after the quench in $g = 0$ calculated numerically for $\tau_Q = 800$.

The ferromagnetic spin-spin correlation function is more interesting since it measures correlations in order parameter:

$$C_R^{xx} = \langle \sigma_n^x \sigma_{n+R}^x \rangle - \langle \sigma_n^x \rangle \langle \sigma_{n+R}^x \rangle = \langle \sigma_n^x \sigma_{n+R}^x \rangle \tag{2.33}$$

The fully analytical calculations are much more daunting here and in most cases simply impossible. It is well known that in the ground state C_R^{xx} can be written as a determinant of an $R \times R$ Toeplitz matrix whose asymptote for large R can be obtained with the Szego limit theorem, see Appendix C. Unfortunately, in time-dependent problems the correlation function is not a determinant in general. However, below we will avoid this problem in an interesting range of parameters obtaining analytical results. In order to get

a full picture, we will supplement those results by numerical studies for arbitrary values of parameters both after the quench in $g = 0$ and in the middle of the quench $g = 1$.

Using the Jordan-Wigner transformation (A.3), C_R^{xx} can be expressed as

$$C_R^{xx} = \langle b_0 a_1 b_1 a_2 \dots b_{R-1} a_R \rangle \ . \tag{2.34}$$

Here a_n and b_n are Majorana fermions defined as $a_n = c_n^\dagger + c_n$ and $b_n = c_n^\dagger - c_n$. Using (2.27) we get:

$$\begin{aligned} \langle a_m b_n \rangle &= 2\alpha_{n-m} + 2\Re\beta_{n-m} - \delta_{m,n} \\ \langle b_m a_n \rangle &= \delta_{m,n} - 2\alpha_{n-m} + 2\Re\beta_{n-m} \\ \langle a_m a_n \rangle &= \delta_{m,n} + 2\imath\Im\beta_{m-n} \\ \langle b_m b_n \rangle &= \delta_{m,n} + 2\imath\Im\beta_{m-n} \end{aligned} \tag{2.35}$$

The average in Eq. (2.34) can be expressed as a Pfafian of the antisymetric matrix:

$$|C_R^{xx}| = |Pf[A_R^{xx}]| \tag{2.36}$$

where

$$A_R^{xx} = \left[\begin{array}{cc} \langle a_{m+1} a_{n+1} \rangle & \langle b_m a_{n+1} \rangle \\ \langle a_{m+1} b_n \rangle & \langle b_m b_n \rangle \end{array} \right]_{m,n=1,\dots,R} . \tag{2.37}$$

We redefine here $\langle a_n a_n \rangle = \langle b_n b_n \rangle = 0$ so that A_R^{xx} is antisymmetric. This can be seen when we we use Wick theorem and realize that different Majorana fermions anticommutate. Using textbook properties of Pffafian this means that:

$$|C_R^{xx}| = \sqrt{|\det A_R^{xx}|} \tag{2.38}$$

determining correlation function up to the sign factor. A_R^{xx} is block 2Rx2R Toeplitz matrix but we were not able to find the determinant in that case analytically.

In order to get some analytical predictions we can notice that when $\langle a_m a_n \rangle = 0$ and $\langle b_m b_n \rangle = 0$ for $m \neq n$, or equivalently when $\Im\beta_{m-n} = 0$ for $m \neq n$ then expression for C_R^{xx} take simpler form

$$C_R^{xx} = \det \left[\langle b_m a_{n+1} \rangle \right]_{m,n=1,\dots,R} \ . \tag{2.39}$$

Inspection of the last line in Eq. (2.29) shows that $\Im\beta_{m-n} \approx 0$ when $|m - n| \ll l$. Consequently, when the correlation distance $R \ll l$ we can neglect all $\Im\beta_{m-n}$ assuming that $\langle a_m a_n \rangle = 0$ and $\langle b_m b_n \rangle = 0$ for $m \neq n$.

Asymptotic behavior of this Toeplitz determinant $\det \left[\langle b_m a_{n+1} \rangle \right]_{m,n=1,\dots,R}$ can be obtained using standard methods (see Appendix C) with the result that

$$C_R^{xx} \sim \exp\left(-0.174 \, \frac{R}{\hat{\xi}} \right) \cos\left(\sqrt{\frac{\log 2}{2\pi}} \, \frac{R}{\hat{\xi}} - \varphi \right) \tag{2.40}$$

when $1 \ll R \ll l$.

In this way we find that the final ferromagnetic correlation function at $g = 0$ exhibits decaying oscillatory behavior on length scales much less than the phase - ordered scale l, but both the wavelength of these oscillations and their exponentially decaying envelope

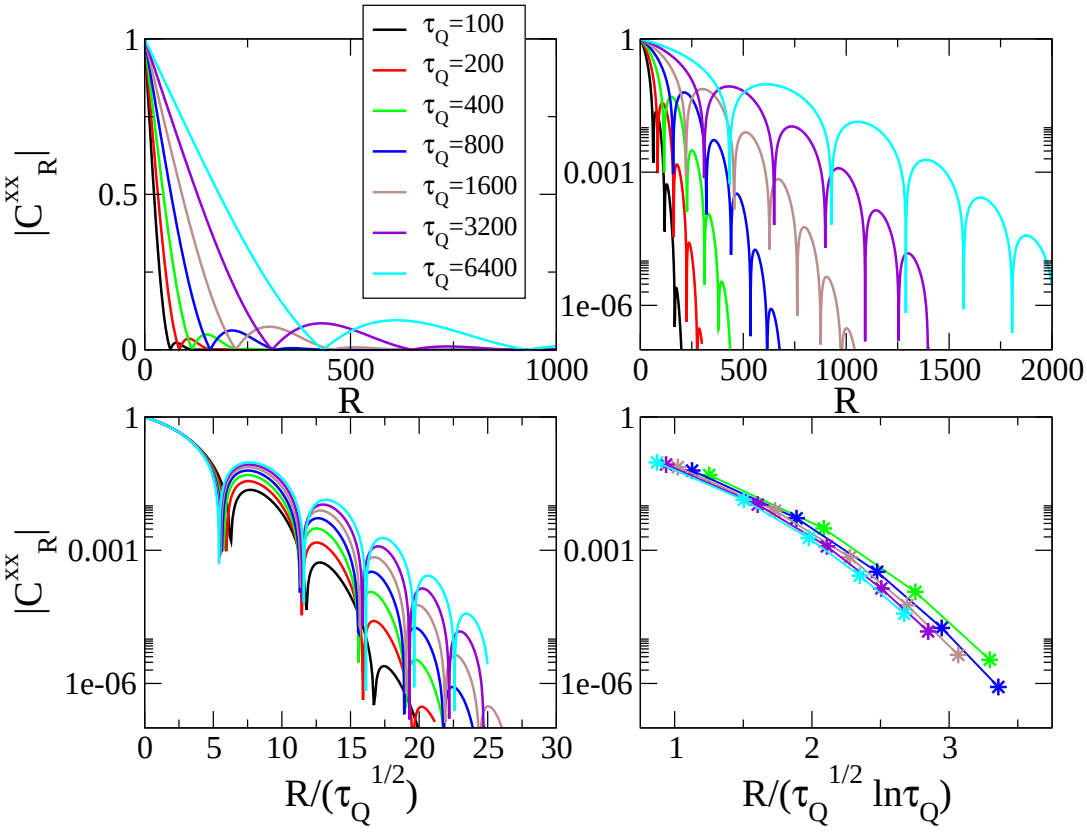

Figure 2.2: Numerical calculation of correlation function C_R^{xx} after the quench in g=0 for several values of τ_Q. In Panel A and B C_R^{xx} in linear and logarithmic scale. In Panel C: C_R^{xx} with R rescaled by $\hat{\xi}$. For small R curves nearly collapse in agreement with (2.40). For large R the curves do not longer colapse - C_R^{xx} decays slower then on R but oscillations keep the wavelength roughly $\sim \hat{\xi}$. In Panel D local maxima of oscilations from Panel A for R rescaled by l. The curves nearly collapse onto each other suggesting that for large distance R correlations C_R^{xx} decays on the length scale set by l.

are determined by $\hat{\xi}$. As discussed in a similar situation [34], this oscillatory behavior means that consecutive kinks are approximately anticorrelated – they keep more or less the same distance $\simeq \hat{\xi}$ from each other forming something similar to a ...-kink-antikink-kink-antikink-... lattice with a lattice constant $\simeq \hat{\xi}$.

The analytical results are, however, limited to R such that $1 \ll R \ll l$. To obtain the tail of the correlation function we need to use full expression for ferromagnetic correlations in Eq. (2.38). The results are shown on Fig. 2.2. We calculate α_n and β_n in (2.27) numerically integrating full expression for Bogoliubov modes (Appendix B). In Fig. 2.2 A we see that C_R^{xx} indeed shows oscillatory behavior and in Panel B we see the same plot in logarithmic scale. Dips represent places where C_R^{xx} crosses zero. Panel C shows correlation function when R was rescaled by $\hat{\xi}$ as in analytic (2.40). The wavelength of oscillations is roughly determined by $\hat{\xi}$. We see as well, that for smaller R and larger τ_Q the plots nearly collapse onto each other as pedicted by (2.40). However when R gets larger and condition $R \ll l$ no longer applies we see that the correlation decay faster then

on the length scale $\hat{\xi}$. In order to estimate it in Panel D we plot local maxima of C_R^{xx} (to get rid of oscillatory behavior) and plot then on the length scale given by l. The collapse is far from perfect but for larger τ_Q the rescaled curves are close to each other suggesting that for $R \gg l$ the ferromagnetic correlation functions decay exponentially on the length scale given by l which is larger then $\hat{\xi}$.

2.3.2 Correlations during the quench

To get a better picture we turn to studying correlation function during the quench at $g = 1$. It is not known how to expand Bogoliubov model (u_k, v_k) in Appendix B when $g = 1$ and we must rely on numerical results. Correlations in the direction of the field C_R^{zz} are shown in Fig. 2.3

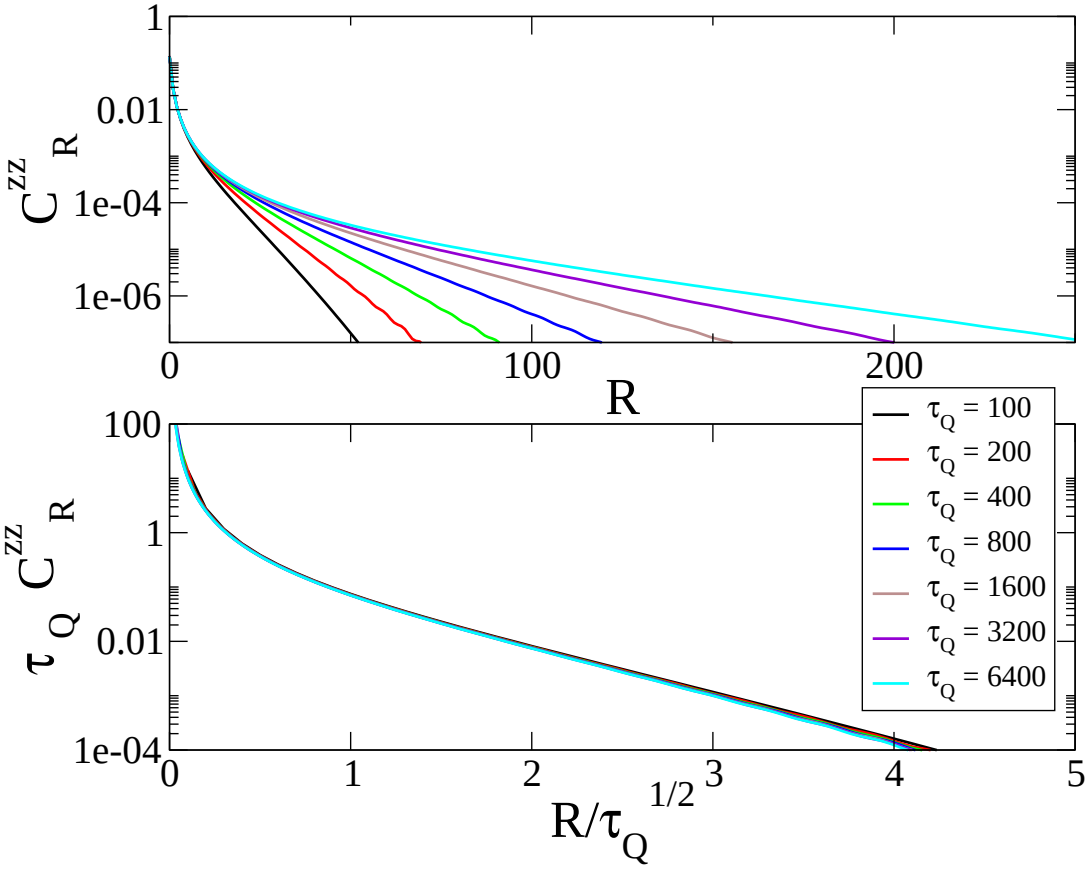

Figure 2.3: Numerical results for correlation function C_R^{zz} during the quench at g=1 for several values of τ_Q. The rescaled curves in Panel B suggest that the correlation are describet by Eqs. (2.41) and $\hat{\xi}$ is the only relevant scale of length.

In Fig. 2.3 A we plot C_R^{zz} in logarithmic scale for sevaral values of quench rate τ_Q. In panel B the correlations has been a properly rescaled by Kibble-Zurek correlation length $\hat{\xi}$. The curves nearly collapse onto each other. We can fit the following behavior:

$$C_R^{zz} \approx \frac{0.44}{\tau_Q} \exp\left(-2.03\frac{R}{\hat{\xi}}\right) \tag{2.41}$$

accurate when $R \gg \hat{\xi}$. This tail decays exponentially on the Kibble-Zurek correlation length $\hat{\xi}$ which proves to be the only relevant scale of length.

Similarly we can look at ferromagnetic correlations C_R^{xx} plotted in Fig. 2.4. Surprisingly the correlations decays faster then exponentially here (see Fig. 2.4 A). On the other hand when we rescale R by $\hat{\xi}$ the curves nearly collapse – especially for larger τ_Q again showing that at the critical point we only have one relevant correlation length $\hat{\xi}$ which we attribute to universal Kibble-Zurek mechanism.

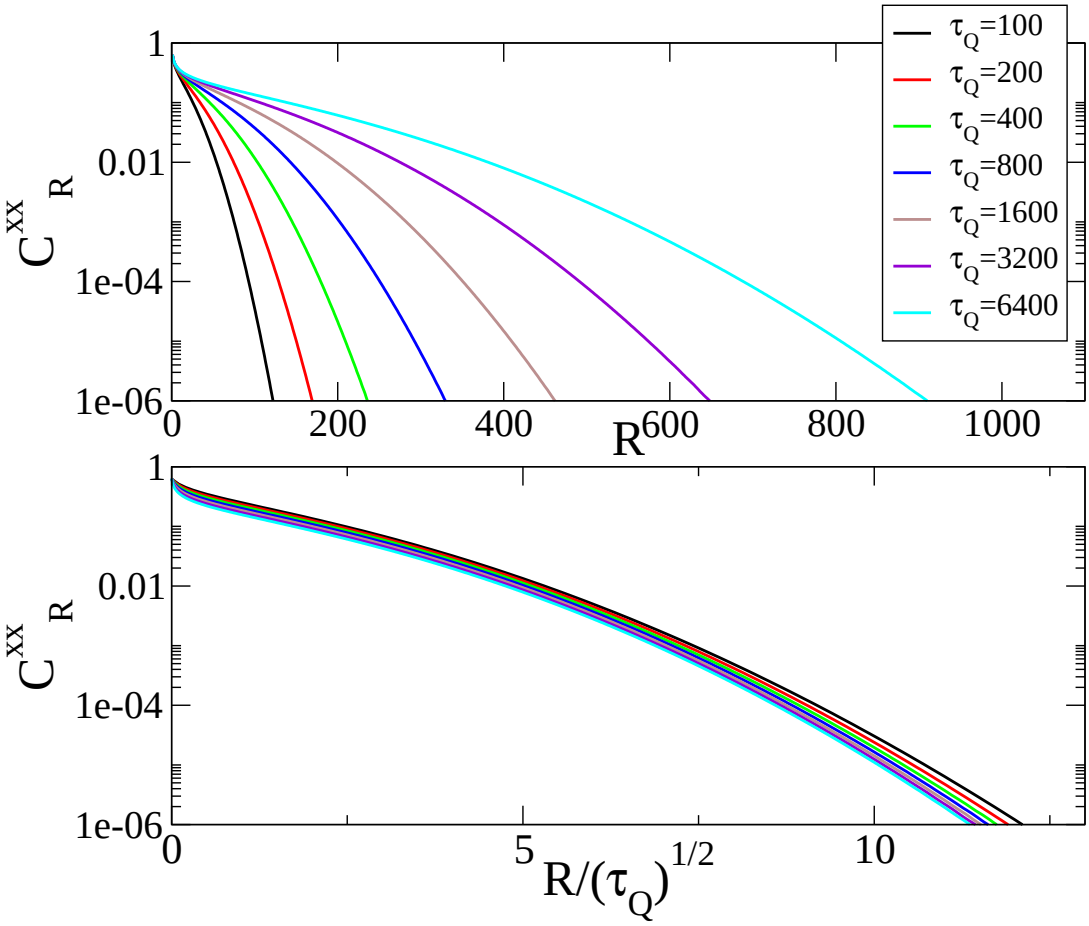

Figure 2.4: Numerical calculations for correlation function C_R^{xx} during the quench in g=1 for several values of τ_Q. The rescaled curves in Panel B roughly collapse onto each other suggesting that $\hat{\xi}$ is the only revelant length scale here.

2.4 Fidelity

Quantum fidelity – also referred to as fidelity – is a popular measure of closeness of two quantum states coming from quantum information science [35]. For the pure states – as in our case – it simplifies to the overlap between two quantum states, or equivalently – for probabilistic interpretation reasons – square of the overlap. We will use the latter definition:

$$\mathcal{F} = |\langle \psi(0) | g = 0 \rangle|^2 \tag{2.42}$$

Here we calculate fidelity between final state after evolution $|\psi(0)\rangle$ when $g = 0$ and the ground state at $|g = 0\rangle$.

From (2.14) we get

$$\mathcal{F} = \Pi_{k>0}|A_k|^2 \tag{2.43}$$

or equivalently

$$\ln \mathcal{F} = \sum_{k>0} \ln(1 - p_k) = \frac{N}{2\pi} \int_0^\pi dk \ln(1 - e^{-2\pi\tau_Q k^2}) \tag{2.44}$$

in the limit of large system size and slow transition $\tau_Q \gg 1$ (still $\tau_Q \ll N^2$ as opposed to 'adiabatic limit' (2.24)). This gives:

$$\ln \mathcal{F} \simeq \frac{N}{2\pi\sqrt{2\pi\tau_Q}} \int_0^\infty dl \ln(1 - e^{-l^2}) \simeq -\frac{1.306N}{2\pi\sqrt{2\tau_Q}} \simeq -1.306Nd \tag{2.45}$$

where n is density of excitations after the quench (2.21).

On the other hand fidelity defined as a overlap of two statical quantum ground states calculated for slightly different values of parameter was recognize recently as a good indication of quantum criticality. It follows the discovery that quantum criticality points promotes decay of fidelity [36]. We have studied the fidelity in that context in the thermodynamic limit [VII] and shown – among others – that in case of the Ising model

$$\ln \ \langle 1 + \delta|1 - \delta\rangle \simeq -\frac{1}{4}N\delta. \tag{2.46}$$

in the leading order in δ. The thermodynamic limit is reached here when size of the system N is large enough when compared with δ i.e. $N\delta \gg 1$. In the opposite limit $N\delta \ll 1$ we have to take into account finite size effects and the fidelity $\ln \ \langle 1 + \delta|1 - \delta\rangle \simeq -\frac{1}{16}N^2\delta^2$.

Following the adiabatic-impulse-adiabatic approximation (sec. 2.1) we notice that we should expect that fidelity after the transition is equal to fidelity between states $|+\hat{\epsilon}\rangle$ and $|-\hat{\epsilon}\rangle$ (2.5). Indeed as described in sec. 2.1 when we assume, that state $|+\hat{\epsilon}\rangle$ is – with a good approximation – an initial state for subsequent adiabatic evolution starting at $|-\hat{\epsilon}\rangle$ then the probability that the state of the system is in the -instantaneous - ground state should not change and is $|\langle+\hat{\epsilon}|-\hat{\epsilon}\rangle|^2$. This - taking into account (2.5) and (2.46) gives us

$$\ln \mathcal{F} \sim -N\frac{1}{\sqrt{\tau_Q}}. \tag{2.47}$$

in agreement with (2.45). We should point out here that we do not expect to have a sharp boarder between adiabatic and impulse regime and additionally (2.5) is expected to be given up to the $\mathcal{O}(1)$ constant. Still we are able to reproduce the correct scaling behavior in τ_Q providing most direct test of adiabatic-impulse-adiabatic approximation (sec. 2.1).

It is interesting here to discuss the connection between fidelity approach and density of quasiparticles d. However, before we do it that, we should point out some differences showing that although fidelity and density of quasiparticles – as we will see – seems to be closely connected their are not equivalent. In order to do that we have to notice that density of excitations is not always well defined (see e.g. [37]). Let say that in

some arbitrary system we prepare the ground state $|g_1\rangle$ of Hamiltonian $H(g_1)$ and we do the instantaneous quench to $H(g_2)$ with external parameter g_2. In principle we can use density of excitation to describe how much the state of the system is excited. However in nonintegrable systems it, in general, will not be conserved in time after the quench due to various relaxation/colission processes. It is well defined on time scales much shorter then relaxation time. Fortunately for us, all models considered in this thesis are integrable and relaxation time is infinite. On the other hand fidelity $| < g_2|e^{-iH(g_2)t}|g_1 > |$ is constant in time for any – integrable or nonintegrable – Hamiltonian. Because of that it is always well defined and describes the result of quench and not the subsequent evolution.

To establish a connection between density of kinks and fidelity we can consider a simple Poissonian model where each of N bonds is either excited (with probability $d_{\rm exc}$) or not excited (with probability $1-d_{\rm exc}$) *independently* of other bonds. Here $d_{\rm exc}$ is average density of excitations. The fidelity is a probability that none of the N independent bonds is excited

$$\mathcal{F} \;=\; (\; 1 \;-\; d_{\rm exc} \;)^N \;. \tag{2.48}$$

We obtain density of *independent* excitations as

$$d_{\rm exc} \;=\; c\; d \;. \tag{2.49}$$

We can conclude that $c = d_{\rm exc}/d$ measures correlations between kinks: $c < 1$ means bunching and an eventual $c > 1$ would mean anti-bunching of kinks randomly distributed along the spin chain. For the Ising model $c \simeq 1.3$ which means anti-bunching of kinks. This can be also seen in ..-kink-antikink-king-.. structure of ferromagnetic correlation function after the quench, see Fig. 2.2.

2.5 Conclusion

In this chapter we have studied linear homogenous quench in the quantum Ising model. The results are in full agreement with Kibble-Zurek mechanism. We discussed the behavior of fidelity and correlation functions. After the transition we are able to identify two characteristic scales of length. One is the $\hat{\xi}$ – characteristic for universal Kibble-Zurek mechanism. Second, a somewhat larger lengthscale l appears due to subsequent nonuniversal evolution of (excited) state in the ferromagnetic phase. It develops as a result of a dephasing process that can be regarded as a quantum analogue of phase ordering. On the other hand the state of the system during the transition exhibit only characteristic lengthscale $\hat{\xi}$. Indeed there is no time for the (just) excited state to evolve and develop other – nonuniversal – lengthscales. Those results are further corroborated by the studies of entropy of entanglement – which are not discussed in this thesis and can be found in [I].

Chapter 3

Inhomogeneous quench

In a realistic experiment it is usually difficult to make an external parameter ϵ – or other parameters determining Hamiltonian – homogeneous throughout the system. It is especially true in ultracold atom gases in magnetic/optical traps, see e.g. [3]: a trapping potential results in inhomogeneous density of atoms $\rho(\vec{r})$ and a critical properties of the system usually depends on atomic density ρ. For example in a Bose-Einstein condensate in an optical lattice [38, 39] we observe a spatial structure of plateaus of Mott insulator phases with different filling separated by thin layers of superfluid.

In context of finite temperature dynamical transition a good example is provided by superfluid ^3He experiments [14, 15] where the transition was caused by neutron irradiation of helium 3. Heat released in each fusion event, $n + {}^3He \rightarrow {}^4He$, created a bubble of normal fluid above the superfluid critical temperature T_c. As a result of quasiparticle diffusion, the bubble was expanding and cooling with local temperature $T(t,r) = \exp(-r^2/2Dt)/(2\pi Dt)^{3/2}$, where r is a distance from the center of the bubble and D is a diffusion coefficient. Since this $T(t,r)$ is hottest in the center, the transition back to the superfluid phase is driven by an inhomogeneous parameter

$$\epsilon(t,r) \;=\; \frac{T(t,r)-T_c}{T_c}\;.$$

It proceeded from the outer to the central part of the bubble with a critical front $r_c(t)$, where $\epsilon = 0$, shrinking with a finite velocity $v = dr_c/dt < 0$. In such a context the dynamical process was studied in [40, 41, 42] with the results that number of topological defects is drastically suppressed when the velocity with which the (local temperature) quench propagates falls below some threshold velocity. This threshold is approximately given by the ratio of the healing length to relaxation time at freeze-out, which is the instant when the critical slowing down results in a transition from the adiabatic to the impulse behavior.

In this chapter we will provide the general argument predicting when the smooth spatial inhomogeneity is and when it is not relevant for the dynamical transition across the quantum critical point. Indeed we will see that when the transition velocity is large enough then inhomogeneity is not of the great importance and the system gets excited as predicted by (homogeneous) Kibble-Zurek mechanism. On the other hand, when we cross the critical point with small enough velocity then it turns out that we are able to do it in an almost adiabatic manner. This may be of great importance in adiabatic state

preparation mentioned in the Introduction. Those predictions will be illustrated using two models. One is the quantum Ising chain – which we have studied in detiles in the homogeneous case in the previous Chapter – and the second is a specific case of XY model with dynamical exponent $z > 1$. Such choice (dynamical exponent z>1) allows for some additional nontrivial effects not present when $z = 1$ (like in the Ising model).

This chapter compiles and complements results published in [III, IV].

3.1 Large velocity limit and Kibble-Zurek mechanism

We have discussed the Kibble-Zurek mechanism in sec. 2.1. It predicts that in a homogeneous symmetry breaking transition, a state after the transition is a mosaic of finite ordered domains of average size $\hat{\xi}_{KZ}$. Within each finite domain orientation of the order parameter is (in first approximation) constant but uncorrelated to orientations in other domains. In contrast, in an inhomogeneous symmetry breaking transition [40, 41, 42], the parts of the system that cross the critical point earlier may be able to communicate their choice of orientation of the order parameter to the parts that cross the transition later and bias them to make the same choice. Consequently, the final state may be correlated at a range longer than $\hat{\xi}_{KZ}$ or even end up being the ground state. Namely the final density of excited quasiparticles may be lower than the Kibble-Zurek estimate in Eq. (2.7) or even end up equal to zero.

From the point of view of testing Kibble-Zurek, this inhomogeneous scenario, when relevant, may sound like a negative result because an imperfect inhomogeneous transition suppresses Kibble-Zurek mechanism. However, from the point of view of adiabatic quantum computation or adiabatic quantum state preparation it is the Kibble-Zurek mechanism itself that is a negative result: no matter how slow the homogeneous transition is there is a finite density of excitations (2.7) which decays only as a fractional power of transition time τ_Q. From this perspective, the inhomogeneous transition may be a practical way to suppress Kibble-Zurek excitations and prepare the desired final ground state adiabatically.

To estimate when the inhomogeneity may actually be relevant and to define a problem in an unambiguous way, similarly to Eq. (2.2), we linearize the parameter $\epsilon(t, n)$, which is driving the transition, in both n and t near the critical front where $\epsilon(t, n) = 0$ as

$$\epsilon(t, n) \approx \alpha\ (n - vt)\ . \tag{3.1}$$

Here n is position in space, e.g. lattice site number, α is a gradient (degree of inhomogeneity) of the transition, and v is velocity of the critical front. When watched locally at a fixed n, the inhomogeneous transition in Eq. (3.1) appears to be the homogeneous transition in Eq. (2.2) with a local quench time

$$\tau_Q = \frac{1}{\alpha v}\ . \tag{3.2}$$

The part of the system where $n < vt$, or equivalently $\epsilon(t, n) < 0$, is already in the broken symmetry phase. In principal, an outcome of the transition should depend on v.

On the one hand, there cannot be efficient communication across the critical point when the front is moving faster than quasiparticles near the critical point:

$$v \gg v_q\ . \tag{3.3}$$

Here v_q is the maximal group velocity of quasiparticles at $\epsilon = 0$ or, in general, a Lieb-Robinson velocity [43]. It is a constant that does not depend on the inhomogeneity α. In this "homogeneous regime" the inhomogeneous transition is effectively homogeneous and the final density of excitations after the transition is given by Eq. (2.7) with the local $\tau_Q = 1/\alpha v$. In some cases we might expect (3.3) to be too strong a condition. The maximum velocity of the quasiparticles v_q might be defined for quasiparticles which do not get excited during transition. In the same time quasiparticles which do get excited might have smaller group velocity.

On the other hand, Kibble-Zurek mechanism provides the relevant scales of length and time, $\hat{\xi}_{KZ}$ and $\hat{t}_{KZ}$ (through the inverse of the energy gap at $\hat{\epsilon}_{KZ}$) respectively, whose combination [40, 41, 42]

$$\hat{v} \simeq \frac{\hat{\xi}_{KZ}}{\hat{t}_{KZ}} \sim \alpha^{\frac{\nu(z-1)}{1+\nu}} . \tag{3.4}$$

is a relevant scale of velocity. Here we used Eqs. (2.5), (2.6) and (3.2) which is valid for small α. Indeed, when

$$v \gg \hat{v} \tag{3.5}$$

the system does not have enough time to adjust on the relevant length scale $\hat{\xi}_{KZ}$ and the density of excitations should be equall to the homogeneous case (2.7). When the above condition is not longer valid we can expect that prediction coming from (homogenous) Kibble-Zurek mechanism should break.

The two conditions (3.3) and (3.5) are equivalent when dynamical exponent $z = 1$. Indeed in that case we have well defined (one) velocity of quasiparticles near the critical point which is a constant independent from α. For $z > 1$ the obtained results (as shown below for specific case of XY model) turn out to be ambiguous and are not strong enough a proof to claim that the weaker condition (3.5) (for z>1) is sufficent.

3.2 Small velocity limit and Kibble-Zurek mechanism is space

References [44, 45, 46] considered a "phase transition in space" where $\epsilon(n)$ is inhomogeneous but time-independent. In the same way as in Eq. (3.1), this parameter can be linearized as near the critical front $\epsilon(n_c) = 0$ as

$$\epsilon(n) \simeq \alpha\ (n - n_c) . \tag{3.6}$$

The system is in the broken symmetry phase where $n < n_c$ and in the symmetric phase where $n > n_c$. In the first "local approximation", we would expect that the order parameter behaves as if the system were locally homogeneous: it is nonzero for $n < n_c$ only, and when $n \to n_c^-$ it tends to zero as $(n_c - n)^\beta$ with the critical exponent β. However, this first approximation is in contradiction with the basic fact that the correlation length ξ diverges near the critical point and the diverging ξ sets the shortest length scale on which the order parameter can adjust to the changing $\epsilon(n)$. Consequently, when approaching n_c^- the local approximation $(n_c - n)^\beta$ must break down. It happens when the local correlation

length is equal to length scale at which the critical point is approached

$$\frac{1}{|\epsilon(n)|^{\nu}} \sim \frac{|\epsilon(n)|}{|\frac{d}{dn}\epsilon(n)|}, \tag{3.7}$$

compare with similar argument in (2.3). Solving this equality with respect to n, we obtain

$$n_{SP} - n_c \ \sim \ \alpha^{-\frac{\nu}{1+\nu}} \ . \tag{3.8}$$

or equivalently

$$\hat{\xi}_{SP} \ \sim \ \alpha^{-\frac{\nu}{1+\nu}} \ . \tag{3.9}$$

In other words, beginning from $n - n_c \simeq -\hat{\xi}_{SP}$ the "evolution" of the order parameter in n becomes "impulse", i.e, in the 'zero order approximation' the order parameter does not change until $n - n_c \simeq +\hat{\xi}_{SP}$ in the symmetric phase, where it begins to follow the local $\epsilon(n)$ again and decays to zero on the same length scale of $\hat{\xi}_{SP}$.

A direct consequence of this "KZM in space" is that a non-zero order parameter penetrates into the symmetric phase to a depth

$$\delta n \ \sim \ \hat{\xi}_{SP} \tag{3.10}$$

as if the the critical point were effectively "rounded off" on the length scale of $\hat{\xi}_{SP}$. We expect that this rounding-off results also in a finite energy gap which scales as

$$\hat{\Delta}_{SP} \ \sim \ \hat{\xi}_{SP}^{-z} \ \sim \ \alpha^{\frac{z\nu}{1+\nu}} \tag{3.11}$$

in contrast to the local approximation, where we would expect gapless excitations near the critical point. This finite gap should prevent excitation of the system even when the critical point n_c in Eq. (3.6) moves with a (small) finite velocity: $n_c(t) = vt$. The excitation is suppressed up to a threshold velocity

$$\hat{v} \ \simeq \ \frac{\hat{\xi}_{SP}}{\hat{\Delta}_{SP}^{-1}} \ \sim \ \alpha^{\frac{\nu(z-1)}{1+\nu}} \tag{3.12}$$

which is a ratio of the relevant length $\hat{\xi}_{SP}$ to the relevant time $\hat{\Delta}_{SP}^{-1}$. This defines 'inhomogenouse regime' of transition where we are able to cross the critical point without collectively exciting the system. We notice that $\hat{v}$ here is the same as Eq. (3.4) obtained from the 'large velocity' limit - but read the remark at the end of section 3.1.

3.3 Ising model

In this section we are going to illustrate and confirm general predictions presented in Sec. 3.1 and 3.2 by studing inhomogenouse transition in the Ising model. The Hamiltonian reads

$$H \ = \ - \ \sum_{n=1}^{N} g_n \ \sigma_n^z \ - \ \sum_{n=1}^{N-1} \sigma_n^x \sigma_{n+1}^x \ . \tag{3.13}$$

where contrary to homogeneous case (2.1), external magnetic field g_n is position dependent and we use open boundary conditions which are more natural in that situation.

Given $z = 1$ and $\nu = 1$ in the homogeneous case, we expect $\hat{v} \simeq 1$ (3.12). More precisely we can find velocity of quasiparticles at the critical point. Given energy spectrum at the critical point $g_c = 1$ (A.12) we easily obtain

$$\hat{v} = v_q = \frac{d\epsilon_k}{dk}|_{k=0} = 2, \tag{3.14}$$

independent of either τ_Q or α. We notice that maximal group velocity is reached for low lying excitation which – as we will see – get excited when $v > \hat{v}$.

The model is no longer exactly solvable, but still we can obtain some useful analytical insight in the following way.

After Jordan-Wigner transformation (A.3) to spinless fermionic operators c_n, the Hamiltonian (3.13) becomes

$$H \;=\; \sum_{n=1}^{N} g_n \;\left(2c_n^\dagger c_n - 1\right) - \sum_{n=1}^{N-1} \left(c_n^\dagger c_{n+1} + c_{n+1} c_n + \text{h.c.}\right), \tag{3.15}$$

see (A.6) for comparison. The model is no longer translationally invariant and in principle Fourier transform does not diagonalize (3.15). In order to diagonalize this quadratic Hamiltonian to

$$H = \sum_m \omega_m \gamma_m^\dagger \gamma_m + \text{const}$$

we use a full (2N x 2N) Bogoliubov transformation

$$\begin{aligned} c_n &= \sum_{m=0}^{N-1} (u_{nm}\gamma_m + v_{nm}^* \gamma_m^\dagger), \\ c_n^\dagger &= \sum_{m=0}^{N-1} (u_{nm}^* \gamma_m^\dagger + v_{nm}\gamma_m), \end{aligned} \tag{3.16}$$

with m numerating N eigenmodes of stationary Bogoliubov-de Gennes equations

$$\omega_m u_{n,m}^{\pm} = 2g_n u_{n,m}^{\mp} - 2u_{n\mp1,m}^{\mp} \tag{3.17}$$

with $\omega_m \geq 0$. For simplicity, we use notation where $u_{nm}^{\pm} \equiv u_{nm} \pm v_{nm}$.

We notice here that the Hamiltonian (3.13) commutes with a parity operator

$$P \;=\; \prod_{n=1}^{N} \sigma_n^z \;=\; \prod_{n=1}^{N} \left(1 - 2c_n^\dagger c_n\right). \tag{3.18}$$

and the even parity of the initial ground state at $\epsilon = 1$ is conserved during the subsequent dynamical transition.

3.3.1 Static solution

We start with finding the ground state of the quantum Ising chain in a static inhomogeneous transverse field g_n which can be linearized near the critical point $g_c = 1$ as

$$\epsilon(n) \;=\; g_n \;-\; 1 \;\approx\; \alpha\,(n - n_c)\;, \tag{3.19}$$

compare with Eq. (3.6). The chain is in the (broken symmetry) ferromagnetic phase where $n < n_c$ and in the paramagnetic phase where $n > n_c$. We want to know if the nonzero ferromagnetic magnetization $X_n = \langle \sigma_n^x \rangle$ in the ferromagnetic phase penetrates across the critical point into the paramagnetic phase and what is the depth δn of this penetration. We are also interested in dependence of excitation gap on α.

Since in a homogeneous system quasiparticle spectrum is gapless at the critical point only, we expect low energy quasiparticle modes $u^{\pm}_{n,m}$ to be localized near the critical point at n_c where we can use the linearization in Eq. (3.19). We also expect that these low energy modes are smooth enough to treat n as continuous and make a long wavelength approximation

$$u^{\mp}_{n\mp 1,m} \approx u^{\mp}_{n,m} \mp \frac{\partial}{\partial n} u^{\mp}_{n,m} \tag{3.20}$$

in Eq. (3.17). Under these assumptions, we obtain a long-wavelength equation

$$\omega_m u^{\pm}_m = 2\alpha(n - n_c) u^{\mp}_m \pm 2\partial_n u^{\mp}_m \ . \tag{3.21}$$

It turns out that the problem is equivalent to harmonic oscillator. Indeed, we introduce rescaled position

$$x \ = \ \sqrt{\alpha}(n - n_c) \ , \tag{3.22}$$

and the eigenmodes can be found as

$$\begin{aligned} u_m(n) \ &\propto \ \psi_{m-1}(x) + \psi_m(x) \ , \\ v_m(n) \ &\propto \ \psi_{m-1}(x) - \psi_m(x) \ , \\ \omega_m \ &= \ \sqrt{8m\alpha} \ , \end{aligned} \tag{3.23}$$

where $\psi_{m\geq 0}(x)$ are eigenmodes of a harmonic oscillator satisfying

$$\frac{1}{2}(-\partial_x^2 + x^2)\psi_m(x) = (m + 1/2)\psi_m(x) \ , \tag{3.24}$$

and $\psi_{-1}(x) = 0$. As expected, the modes in Eq. (3.23) are localized near $n = n_c$ where $x = 0$. A typical width of the lowest energy eigenmodes is $\delta x \simeq 1$, or equivalently

$$\delta n \ \simeq \ \alpha^{-1/2} \ . \tag{3.25}$$

When $\alpha \ll 1$ then $\delta n \gg 1$ and the long wavelength approximation in Eqs. (3.20,3.21) is self-consistent. Thus δn in Eq. (3.25) is the relevant scale of length near n_c and we expect that this δn determines the penetration depth of the spontaneous ferromagnetic magnetization into the paramagnetic phase.

We should stress here that long wavelength approximation and subsequent 'harmonic' modes describing the system holds only for lowest eigenmodes. Hermite function $\psi_m(x)$ becomes highly oscillating as m increases. Indeed $\psi_m(x)$ oscillates on the scale given by $1/\sqrt{m}$. Combining this with (3.22) tells us that the long wavelength approximation holds only for modes with $m \ll 1/\alpha$. Higher energy eigenmode are localized around n where g_n significantly departures from the critical value of the field.

We test this prediction by a numerical solution for an inhomogeneous transverse magnetic field

$$g_n \ = \ 1 + \epsilon_n \ = \ 1 \ + \ \tanh\left[\alpha(n - n_c)\right] \ , \tag{3.26}$$

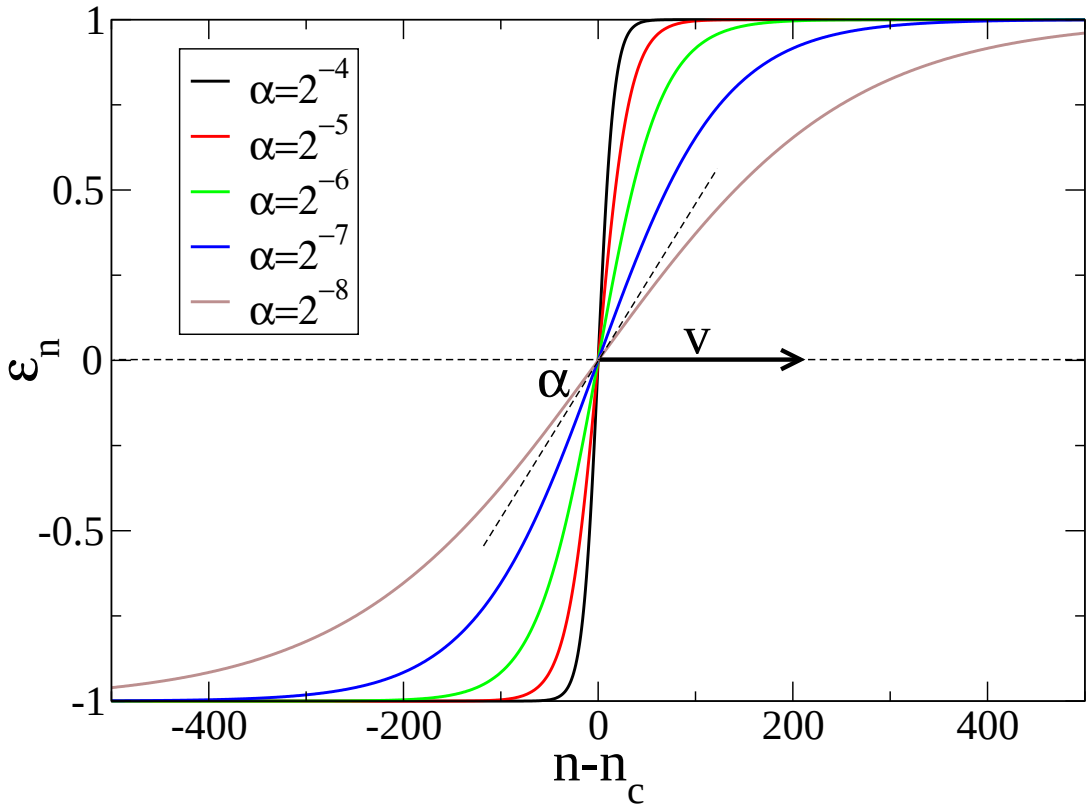

Figure 3.1: The critical front in Eqs. (3.26,3.28).

which is shown in Fig. 3.1 for several values of slope α. This field can be self-consistenly linearized near $n = n_c$ as in Eq. (3.19) because, when the slope $\alpha \ll 1$, the predicted $\delta n \simeq \alpha^{-1/2}$ is much shorter than the width α^{-1} of the tanh. Using such a slant is convenient because away from the critical point when $n = n_c$ the system quickly becomes homogenous and we are able to relate the obtained results to one presented in Chapter 2.

Figures 3.2A and B show how the spontaneous ferromagnetic magnetization $X_n = \langle \sigma_n^x \rangle$ from the ferromagnetic phase, where $n < n_c$, penetrates into the paramagnetic phase, where $n > n_c$. In particular, the collapse of the rescaled plots in Fig. 3.2B demonstrates that the penetration depth is indeed $\delta x \simeq 1$ equivalent to $\delta n \simeq \alpha^{-1/2}$, as predicted in Eqs.(3.10,3.25). Paramagnetic spins near the critical point are biased towards the direction of spontaneous magnetization chosen in the ferromagnetic phase.

Moreover, the analytic solution (3.23) implies a finite relevant (due to conserved parity during evolution) gap

$$\hat{\Delta} \;=\; \omega_0 \;+\; \omega_1 \;=\; \sqrt{8\alpha} \tag{3.27}$$

in accordance with the scaling $\sim \alpha^{1/2}$ predicted by the general Eq. (3.11). This gap is the energy of the lowest excitation of two quasiparticles. We are able to confirm it numerically as well - see Fig. 3.5 A.

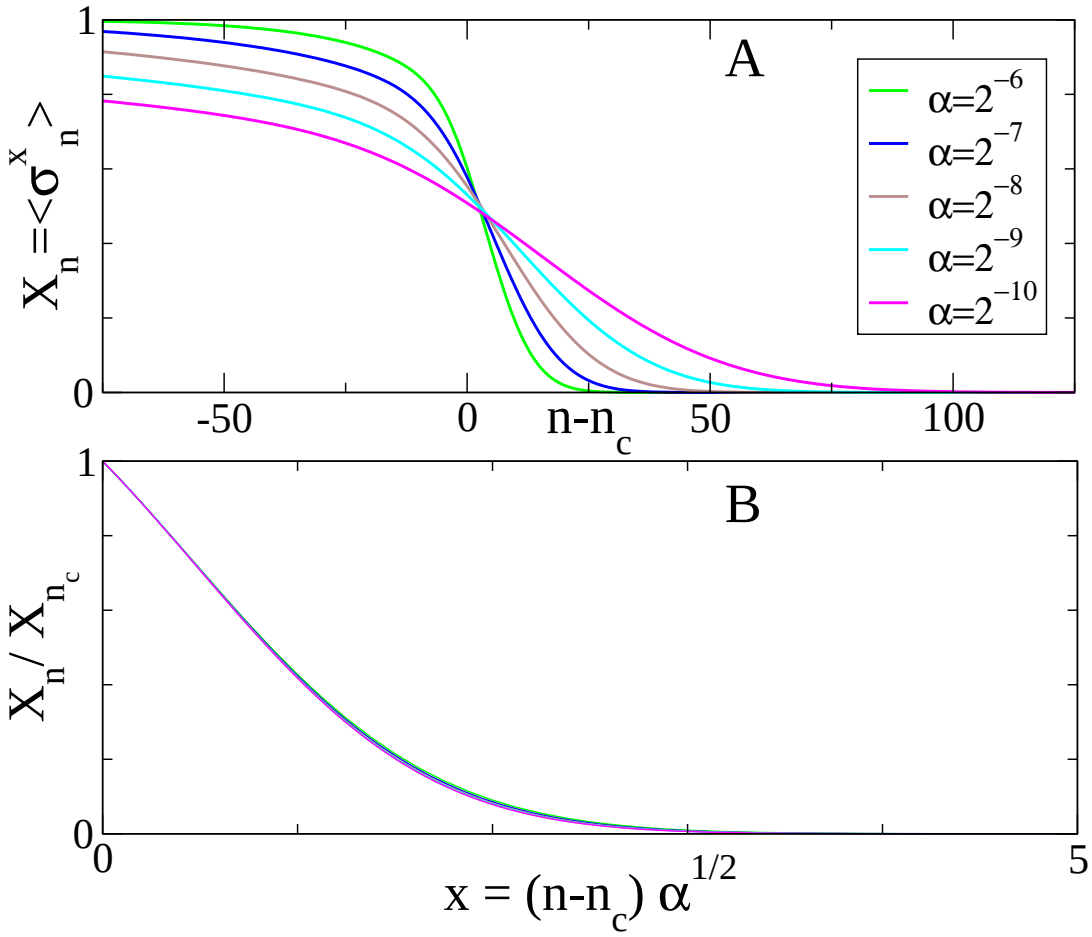

Figure 3.2: Phase transition in space. In A and B, exact numerical spontaneous ferromagnetic magnetization as a function of $n - n_c$ and $x = \sqrt{\alpha}(n - n_c)$ in Eqs. (3.22) respectively. The spontaneous magnetization penetrates into the paramagnetic phase to a depth of $\delta x \simeq 1$, see B, i.e. $\delta n \simeq \alpha^{-1/2}$ in agreement with (3.25) and general (3.10).

3.3.2 Dynamic solution

Let the critical front in Eq. (3.26) and Fig. 3.1 move with a velocity $v > 0$: $n_c(t) = vt$, namely

$$g_n = 1 + \epsilon_n = 1 + \tanh\left[\alpha(n - vt)\right] , \tag{3.28}$$

and we linearize it close to critical value of the magnetic field (3.1)

$$\epsilon(n, t) = g_n - 1 \simeq \alpha(n - vt). \tag{3.29}$$

We proceed in the same way as in homogenous case in Sec 2.2. Time-dependent Bogoliubov method makes an Ansatz that the state of the system is a Bogoliubov vacuum annihilated by a set of quasiparticle annihilation operators $\tilde{\gamma}_k$ defined by a time-dependent

Bogoliubov transformation

$$c_n = \sum_{m=0}^{N-1} \left(u_{nm}(t)\tilde{\gamma}_m + v^*_{nm}(t)\tilde{\gamma}^\dagger_m \right), \tag{3.30}$$
$$c^\dagger_n = \sum_{m=0}^{N-1} \left(u^*_{nm}(t)\tilde{\gamma}^\dagger_m + v_{nm}(t)\tilde{\gamma}_m \right),$$

with the initial condition for $[u_{mn}, v_{mn}]$ given by the solution of static situation calculated for the initial time (3.17). Here we skip index (t) in $[u_{mn}, v_{mn}]$ and whether we are speaking about static or dynamic situation can be understood from the context. In the Heisenberg picture, the Bogoliubov modes must satisfy Heisenberg equation $i\frac{d}{dt}c_n = [c_n, H]$ with the constraint that $\frac{d}{dt}\tilde{\gamma}_m = 0$. The Heisenberg equation gives us the dynamical equivalent of the Bogoliubov-de Gennes equations (3.17):

$$i\partial_t u^\pm_{n,m} = 2g_n u^\mp_{n,m} - 2u^\mp_{n\mp1,m} \tag{3.31}$$

In order to get a long-wavelength version of this equation, which similarly to static case should describe low lying – most relevant during evolution – modes well, we use linearization (3.29) and assume smoothness of the modes in long-wavelength approximation (3.20). We get a time-dependent equivalent of the long-wavelength Eq. (3.21)

$$i\partial_t u^\pm = 2\alpha\,(n - vt)\,u^\mp \;\pm\; 2\partial_n u^\mp\,. \tag{3.32}$$

This equation can be solved exactly for both $v < 2$ and $v > 2$ with qualitatively different solutions in those two regimes. As we have seen $v = 2$ is the (maximal) velocity of quasiparticles at the critical point (3.14) and as explained in Sec. 3.1 3.2 it should be a boarder value between adiabatic-like and Kibble-Zurek like type of behavior.

In order to solve eguation (3.32) when $v < 2$ we change variables to a reference frame co-moving with the front:

$$\bar{t} = t,\; x_v = (n - vt)\left(1 - \frac{v^2}{4}\right)^{-1/4}\sqrt{\alpha} \tag{3.33}$$

and we proceed similarly as for the static case. The solution reads:

$$\begin{aligned} u_m(t,n) &\propto e^{-i\omega_m t}\left[\psi_{m-1}(x_v) + e^{i\varphi}\psi_m(x_v)\right] e^{ivx_v\sqrt{\frac{m}{2}}}\,, \\ v_m(t,n) &\propto e^{-i\omega_m t}\left[e^{i\varphi}\psi_{m-1}(x_v) - \psi_m(x_v)\right] e^{ivx_v\sqrt{\frac{m}{2}}}\,, \\ \omega_m &= \left(1 - \frac{v^2}{4}\right)^{3/4}\sqrt{8\alpha\, m}\,, \end{aligned} \tag{3.34}$$

where $m = 0, 1, 2, ...$, the phase $\varphi = \arcsin(v/2)/2$ and $\psi_m(x)$ are Hermite function (3.24).

When $v \to 0$ we recover the static solutions (3.23). In the reference frame of x_v, which is co-moving with the critical point, the solutions (3.34) are stationary modes with $\omega_m \geq 0$ so we expect no excited quasiparticles in the system after the transition

$$d(v < 2) \;=\; 0\,, \tag{3.35}$$

and, in particular, no kinks where finite $g_n = 0$.

We point out, that solution (3.34) is valid only for low lying modes (small m) with large wave-length, but since such modes do not get excited we have no reason to suspect that modes with larger energy gap should get excited. The solution assumes inadvertently that size of the system $N \to \infty$ to avoid possible problems with boundary conditions. We will see in next subsection that there are possible exponentially small, non-colective excitation, which are independent of system size. There are the result of the critical front leaving (finite) spin chain. They are not registered in (3.35) which is calculated in the limit of infinite system.

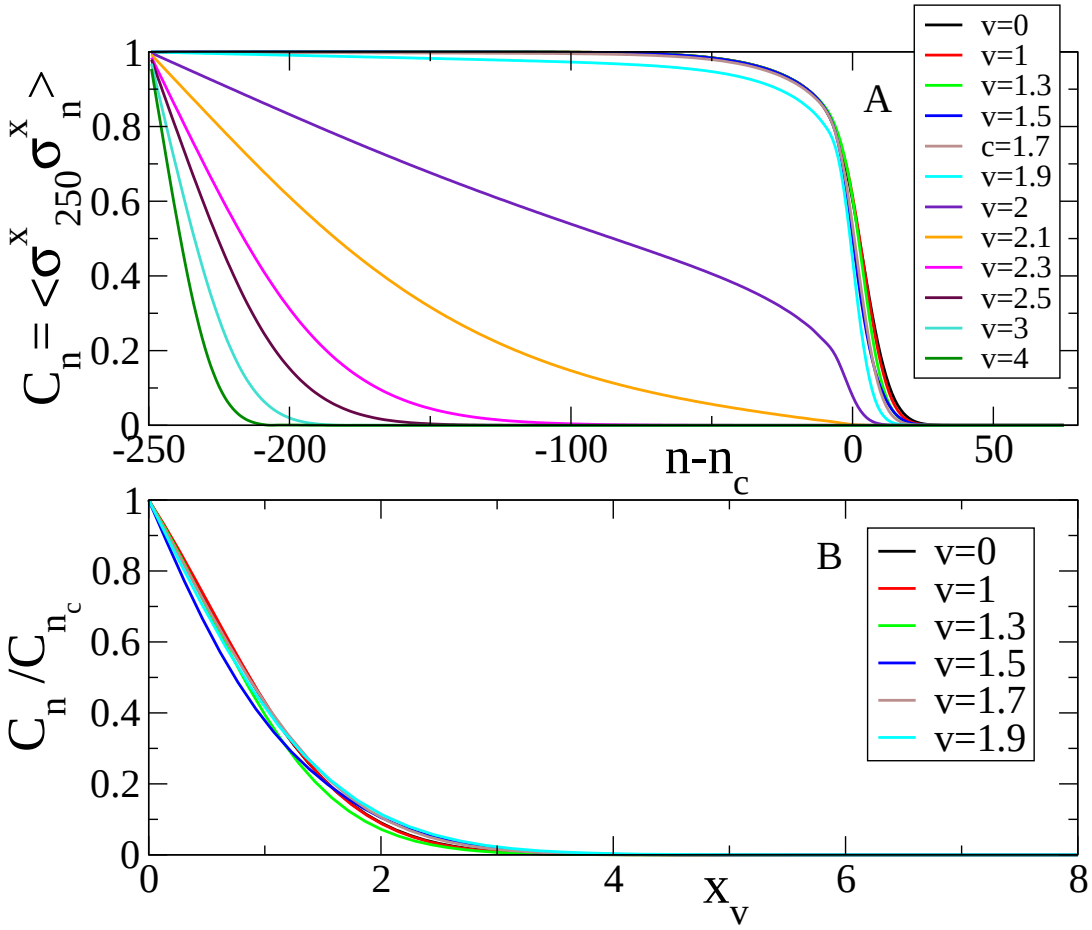

Figure 3.3: Ferromagnetic correlation between the site $n = 250$ in the ferromagnetic phase and a site n when $n_c = vt = 500$ as a function of (A) $n - vt$ and (B) x_v in Eq. (3.33) respectively. Results are obtained for $\alpha = 2^{-6}$ and $N = 600$ using direct numerical evolution of Bogoliubov-de Gennes equation (3.31). When $v \gg 2$ there is no ferromagnetic correlation across the critical point at $n - vt = 0$, see A, and when $v \ll 2$ the correlation penetrates into the paramagnetic phase to a depth of $\delta x_v \simeq 1$, see B.

As shown in Figs. 3.3 B, ferromagnetic correlations penetrate across the critical point

into the paramagnetic phase to a depth $\delta x_v \simeq 1$ equivalent to

$$\delta n_v \;\simeq\; \left(1-\frac{v^2}{4}\right)^{1/4}\; \alpha^{-1/2}\;. \tag{3.36}$$

The penetration depth δn_v shrinks to 0 when $v \to 2^-$ suggesting communication problems across the critical point when, in particularly $v \to 2^-$, and generally $v > 2$.

The same δn_v is a typical width of the lowest eigenmodes in the spectrum (3.34). As it shrinks to 0 when $v \to 2^-$, the eigenmodes become inconsistent with the long-wavelength approximation in Eq. (3.31) and the solution breaks.

On the other hand, in the large velocity limit, when $v > 2$, equation (3.31) can be mapped to a homogeneous transition. Indeed, we change variable to reference frame where magnetic field is constant (in space) for a given point in time.

$$\tilde{t} \;=\; \left(1-\frac{4}{v^2}\right)^{-1}\left(t-\frac{n}{v}\right)\;,\quad \tilde{n} \;=\; n\;, \tag{3.37}$$

Introduced local time $\tilde{t}$ is measured from the moment the critical point passes through n. Simultaneously we make a transformation

$$\begin{pmatrix} u^+ \\ u^- \end{pmatrix} \;=\; \begin{pmatrix} \sqrt{1-\frac{4}{v^2}} & \frac{2i}{v} \\ 0 & 1 \end{pmatrix}\begin{pmatrix} \tilde{u}^+ \\ \tilde{u}^- \end{pmatrix}, \tag{3.38}$$

bringing Eq. (3.32) to a new form (it is convinient here to introduce notation with Pauli matrices):

$$i\partial_{\tilde{t}}\begin{pmatrix} \tilde{u}^+ \\ \tilde{u}^- \end{pmatrix} \;=\; \left[-2\frac{\tilde{t}}{\tilde{\tau}_Q}\sigma^x + 2i\sigma^v\partial_{\tilde{n}} + \frac{4}{iv}\partial_{\tilde{n}}\right]\begin{pmatrix} \tilde{u}^+ \\ \tilde{u}^- \end{pmatrix}\;. \tag{3.39}$$

Here $\sigma^v = \sigma^y\sqrt{1-\frac{4}{v^2}} + \frac{2}{v}\,\sigma^z$ and σ^v is orthogonal to σ^x. Up to an unimportant rotation of a Pauli matrix $\sigma^y \to \sigma^v$ and the momentum-dependent energy shift $\frac{4}{iv}\partial_{\tilde{n}}$, this equation is equivalent to a homogeneous case in Eq. (2.17), but with a longer effective quench time

$$\tilde{\tau}_Q \;=\; \tau_Q\;\left(1-\frac{4}{v^2}\right)^{-3/2} \;>\; \tau_Q. \tag{3.40}$$

In order to show it we do a Fourier transform to quasimomenta representation

$$(\tilde{u}^+,\tilde{u}^-) \;=\; (a_k,b_k)\;\exp(ik\tilde{n}-4ik\tilde{t}/v)/\sqrt{2\pi} \tag{3.41}$$

and bring Eq. (3.39) to the Landau-Zenner form

$$i\frac{d}{d\tau}\begin{pmatrix} a_k \\ b_k \end{pmatrix} \;=\; -\frac{1}{2}(\Delta_k\tau)\;\sigma^x \;+\frac{1}{2}\sigma^v\;\begin{pmatrix} a_k \\ b_k \end{pmatrix}\;, \tag{3.42}$$

where we have rescaled time as $\tau = k\;\tilde{t}$ and $\Delta_k^{-1} = 4\tilde{\tau}_Q k^2$ is a new transition rate – compare with (2.17). The Landau-Zener formula

$$p_k = e^{-\frac{\pi}{2\Delta_k}} = e^{-2\pi\tilde{\tau}_Q k^2}, \tag{3.43}$$

gives excitation probability for a quasiparticle k and density of excited quasiparticles is

$$d(v>2) \;=\; \int_{-\pi}^{\pi} \frac{dk}{2\pi}\, p_k \;=\; \frac{\left(1-\frac{4}{v^2}\right)^{3/4}}{2\pi\sqrt{2\tau_Q}}\,, \tag{3.44}$$

The integral is accurate for $\tilde{\tau}_Q \gg 1$. When $v \gg 2$ the density

$$d(v\gg 2) \;\approx\; \frac{1}{2\pi\sqrt{2\tau_Q}} \;\equiv\; d_{\rm KZM} \tag{3.45}$$

is the same as the density after a homogeneous quench with the same τ_Q, see (2.21), but even for finite $v>2$ d is suppressed below the "homogeneous" density $d_{\rm KZM}$ by the factor $(1-4/v^2)^{3/4}$. The solution breaks when $v \to 2^+$.

The comparison between those results for density of quasiparticles (3.35,3.44) and numerics is very good and is shown in Fig 3.4.

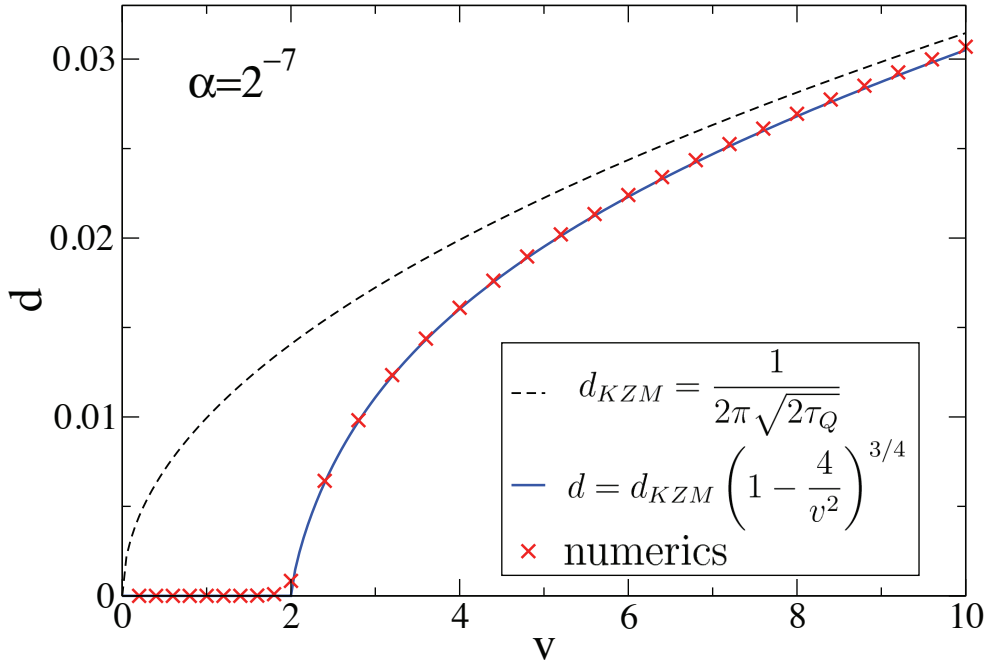

Figure 3.4: Comparison between Eq. (3.44), the homogeneous Kibble-Zurek mechanism, and numerical simulations on a lattice of $N = 400$ spins at a fixed slope $\alpha = 2^{-7}$. The density is calculated near the middle of the chain to avoid boundary effects. $v = 2$ is a critical velocity for which we are not able to avoid such effects fully.

3.3.3 Adiabatic limit

In the previous subsection we have seen that – in the limit of infinite system to avoid boundary effects – we expect no collective excitation when the critical point is crossed

with $v < \hat{v} = 2$. Still it turn out that lowest excited states can have non-negligible excitation probability. We are going to restrict ourselves to the lowest relevant excited state. It turns out to be a very good approximation since probability of exciting next revenant state is exponentially smaller than - already small – probability of exciting the first one.

The state is the even parity state occupied by the lowest two quasiparticles: γ_0 and γ_1. When the critical point n_c is in the bulk of the finite lattice, then these quasiparticles are described by the Bogoliubov-de Gennes modes (3.23) and the energy gap for this excitation is given by Eq. (3.27).

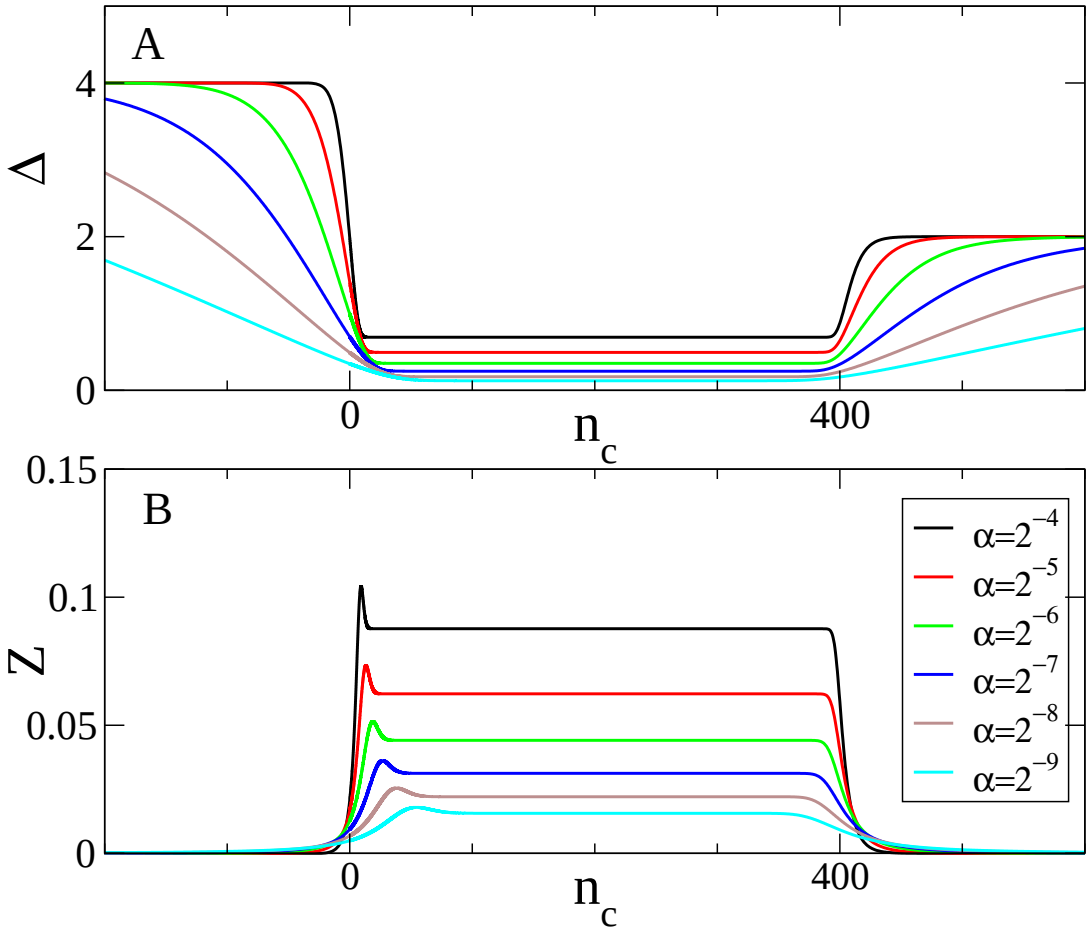

Figure 3.5: Parameters Δ and Z in Landau-Zenner equation (3.47) calculated numerically for a lattice size $N = 400$ and several values of α. In panel A, the instantaneous relevant gap Δ is shown as a function of n_c. The bulk value of the gap, when $1 \ll n_c \ll N$, is estimated in Eq. (3.27) as $\Delta \sim \alpha^{1/2}$. In panel B, the parameter Z in Eq. (3.48) is shown. Its bulk value can be estimated as $Z \sim \alpha^{1/2}$.

In the adiabatic limit we truncate the even parity subspace of the Hilbert space to an effective two-level system:

$$|\psi(t)\rangle \;=\; a(t)\;|0\rangle \;+\; b(t)\;|1\rangle\;, \tag{3.46}$$

where $|0\rangle$ is the instantaneous ground state in the even subspace for an instantaneous position n_c of the critical point and $|1\rangle = \gamma_1^\dagger \gamma_0^\dagger |0\rangle$ is the instantaneous first excited state

for the same n_c. The amplitudes (a, b) satisfy a generalized Landau-Zener problem:

$$i\frac{d}{dt}\begin{pmatrix} a \\ b \end{pmatrix} = \begin{pmatrix} -\Delta/2 & ivZ \\ -ivZ & \Delta/2 \end{pmatrix}\begin{pmatrix} a \\ b \end{pmatrix} \tag{3.47}$$

with initial conditions $a(-\infty) = 1$ and $b(-\infty) = 0$. Here $\Delta = \omega_0 + \omega_1$ is an instantaneous gap and

$$Z \equiv \langle 1|\frac{d}{dn_c}|0\rangle = \sum_{n=1}^{N}(v_{n1}, u_{n1})\frac{d}{dn_c}\begin{pmatrix} u_{n0} \\ v_{n0} \end{pmatrix} . \tag{3.48}$$

Generic $\Delta(n_c)$ and $Z(n_c)$ are shown in Figs. 3.5 A and B respectively.

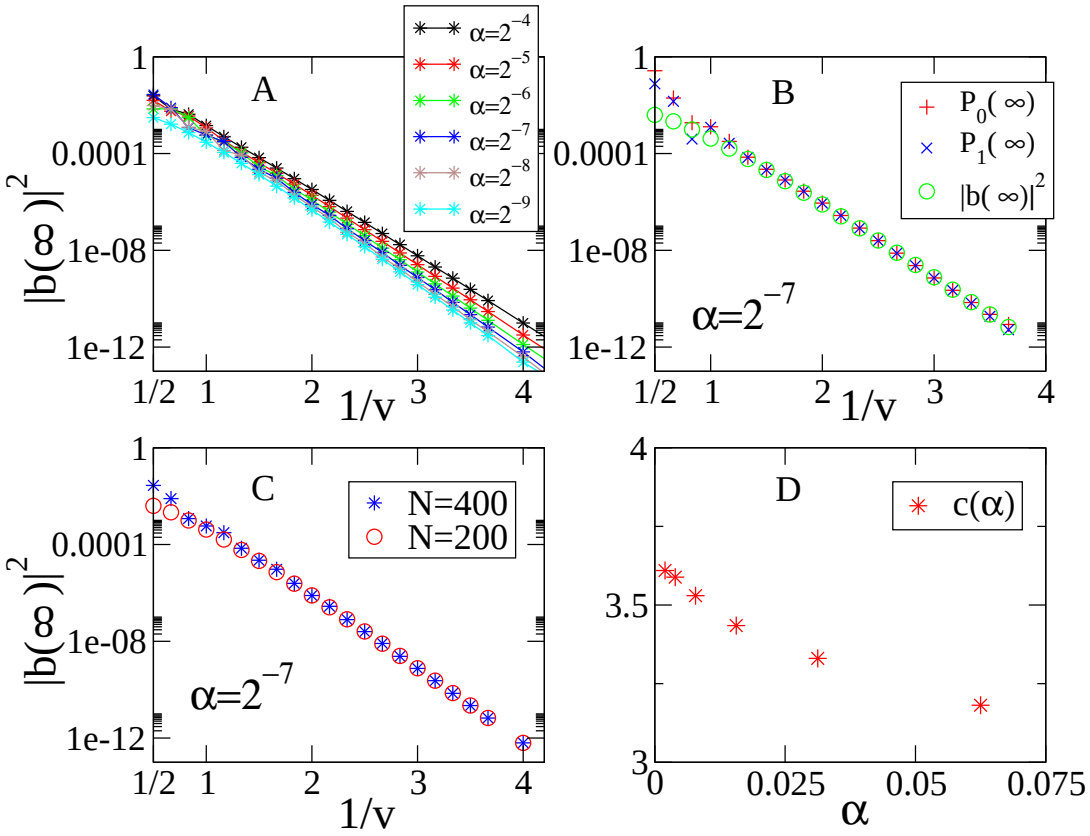

Figure 3.6: Panel A: the final excitation probability $|b(\infty)|^2$ in the generalized Landau-Zener problem (3.47), as a function of $1/v$ for different values of theα and $N = 400$. Panel B, $|b(\infty)|^2$ from the Landau-Zener problem and corresponding excitation probabilities $P_0 = \langle\gamma_0^\dagger\gamma_0\rangle$ and $P_1 = \langle\gamma_1^\dagger\gamma_1\rangle$ from the exact Bogoliubov-de Gennes equations (3.31). All these three probabilities are roughly the same – in the adiabatic regime only a pair of the lowest two quasiparticles γ_0 and γ_1 can get excited. In panel C, $|b(\infty)|^2$ as a function of $1/v$ for a fixed $\alpha = 2^{-7}$ and two different chain sizes $N = 200, 400$. In the adiabatic regime the excitation probability does not depend on N demonstrating that the excitation of the lowest two quasiparticles is a boundary effect In panel D, the coefficients c in (3.49) for several values of α fitted from panel A. When $\alpha \to 0$ then $c \approx 3.7$.

We simulate Landau-Zener equation (3.47) numerically. In the adiabatic limit ($v < 2$) the excitation probability $|b(\infty)|^2 \ll 1$, and the results are well described by a simple Landau-Zener like formula:

$$|b(\infty)|^2 \;=\; \exp\left(-c\,\frac{2}{v}\right)\;, \tag{3.49}$$

where $c = O(1)$ is a numerical prefactor. Indeed, the plots for different α which are collected in Fig. 3.6 A nearly collapse. As shown in Fig. 3.6 D, c has a weak, residual depends on α but when $\alpha \to 0$ then c saturates around $c \approx 3.7$ as assumed in (3.49).

Furthermore, Fig. 3.6 C shows that in the adiabatic regime the small excitation probability $|b(\infty)|^2$ does not depend on the chain size N. Not quite surprisingly, the excitation of the lowest two quasiparticles is a boundary effect determined by the behavior of Δ and Z in Fig. 3.5 when the critical point n_c leaves the chain.

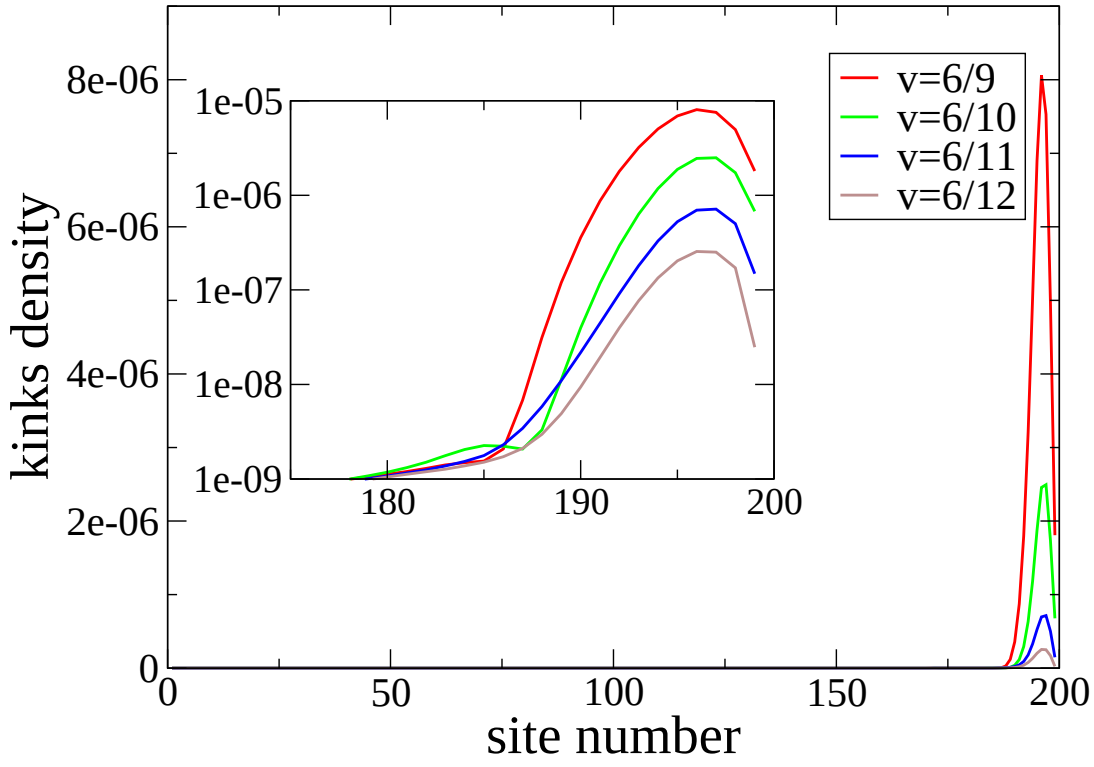

Figure 3.7: Density distributions of kinks along a chain of $N = 200$ spins after an inhomogeneous transition in the adiabatic regime $v < 2$. These distributions were obtained from numerical simulations of the exact time-dependent Bogoliubov-de Gennes equations (3.31) with the critical front in Fig. 3.1. Residual (exponentially small) excitations are brushed away by the critical front to the right edge leaving behind defect-free bulk of the chain. The inset is a log-scale focus on the right edge. It shows that in the adiabatic regime all density distributions for different v look similar up to an overall v-dependent amplitude set by the Landau-Zener excitation probability in Eq. (3.49).

Since the inhomogeneous transition is between two gapped phases, these low frequency modes are localized either near the critical point n_c when n_c is in the bulk of the spin

chain, or at one of the ends of the chain when n_c is near this end. For instance, the "in the bulk" modes in Eqs. (3.23) are localized within the distance $\Delta n \simeq \alpha^{-1/2}$ from the critical point. Consequently, as the critical front in Fig. 3.1 is passing across the chain these instantaneous low frequency modes follow the moving front to the right end of the chain. Indeed, a few generic final density distributions of kinks along the spin chain are shown in Fig. 3.7. These (exponentially small) kink excitations are localized near the right end of the chain. Residual excitations, if any, are brushed away to the right end leaving behind a defect-free bulk of the chain. This is consistent with zero density of kinks in (3.35) calculated for the infinite system (no boundary effects).

3.4 XY multicritical point

In the previous section we studied in details a model with critical exponent $z = 1$. In some sense that is a simple situation. Such value of z means that there is a well defined velocity of quasiparticles at the critical point which is reached for modes with vanishing energy gap. Those are the modes which gets excited during the quench across critical point and, because of that, the critical value of velocity in inhomogeneous transition which is marking the border between adiabatic regime and Kibble-Zurek like regime is a well defined constant independent on degree of inhomogeneity α.

That is why in this section we are going to bring our attentions to situation where $z > 1$ where, for instance, critical value of velocity should depend on α. We are going to study a specific case of the quantum XY spin model - namely the transition across its multicritical point with dynamical exponent $z = 2$. The model turns out to be devious and we cannot – for a reasons outlined in the section and in the end of Appendix A – directly checked predicted scaling laws from Sec. 3.1 and 3.2. Still the model gives us good insight into the dynamics and is worth analyzing.

The Hamiltonian reads:

$$H = -\sum_{n=1}^{N} g_n \sigma_n^z - \sum_{n=1}^{N-1} \left(\frac{1+\gamma_{n+\frac{1}{2}}}{2} \sigma_n^x \sigma_{n+1}^x + \frac{1-\gamma_{n+\frac{1}{2}}}{2} \sigma_n^y \sigma_{n+1}^y \right), \tag{3.50}$$

Where in principle external magnetic field g_n and ferromagnetic spin-spin interaction $(1 \pm \gamma_n)/2$ are position dependent. The homogenous static model is exactly solvable and is discussed in Appendix A. Here we are going to focus on the path in the parameter space $(\gamma, g) = (-\epsilon, 1+\epsilon)$. The parameter ϵ will be driven from the initial $\epsilon = 1$ to the final $\epsilon = -1$, when the Hamiltonian (3.50) becomes the simple Ising chain without magnetic field

$$H_{\text{final}} \;=\; -\sum_{n=1}^{N-1} \sigma_n^x \sigma_{n+1}^x \; . \tag{3.51}$$

The Jordan-Wigner transformation (A.3) translates the the Hamiltonian (3.50) into a free non-interacting fermions model:

$$H \;=\; \sum_{n=1}^{N} (1+\epsilon_n) \; \left(2 c_n^\dagger c_n - 1 \right) - \sum_{n=1}^{N-1} \left(c_n^\dagger c_{n+1} + \epsilon_{n+\frac{1}{2}} c_{n+1} c_n + \text{h.c.} \right), \tag{3.52}$$

which again preserve parity

$$P \;=\; \prod_{n=1}^{N} \sigma_n^z \;=\; \prod_{n=1}^{N} \left(1 - 2c_n^\dagger c_n\right) \;. \tag{3.53}$$

The (infinite) homogeneous system has a second order quantum phase transition (multicritical Lifshitz point) at $\epsilon = 0$, which separates a paramagnetic phase with $\epsilon > 0$ from a ferromagnetic phase where $\epsilon < 0$. We are going to proceed in a similar way as for the Ising chain studied in previous section. However we are not able to obtain such a good analytical insight as for the Ising model and we will be depending heavier on the numerical simulations.

In order to complement the discussion we are going to consider the homogeneous quench first. Then we will focus on inhomogeneous situation by studying both static and dynamic properties.

3.4.1 Homogeneous quench

When $\epsilon_n = \epsilon$ is homogenous throughout the system, it is convenient to use periodic boundary condition and we proceed similarly as in Chapter 2 and Appendix A. We assume that ϵ change in time like

$$\epsilon(t) = -\frac{t}{\tau_Q} \tag{3.54}$$

where τ_Q is the transition rate.

The Fourier transform brings the Hamiltonian into the form (A.9)

$$H^+ \;= \sum_k \Big\{ 2[1 + \epsilon(t) - \cos(k)] c_k^\dagger c_k - \epsilon(t)\, \sin(k) \left[c_k^\dagger c_{-k}^\dagger + c_{-k} c_k \right] - 1 - \epsilon(t) \Big\} \;. \tag{3.55}$$

In order to solve the dynamical problem we use time-dependent Bogoliubov method (discussed in details in Sec. 2.2) where the state of the system is annihilated by fermionic operators $\tilde{\gamma}_k$:

$$\begin{aligned} c_k &= u_k(t)\tilde{\gamma}_k + v_{-k}^*(t)\tilde{\gamma}_{-k}^\dagger \;, \\ c_k^\dagger &= u_k(t)^*\tilde{\gamma}_k^\dagger + v_{-k}(t)\tilde{\gamma}_{-k} \;, \end{aligned} \tag{3.56}$$

and the modes (u_k, v_k) solve time-dependent Bogoliubov equation:

$$\begin{aligned} i\frac{d}{dt}u_k &= +2\left[1 + \epsilon(t) - \cos k\right] u_k - 2\epsilon(t) \sin k \; v_k \;, \\ i\frac{d}{dt}v_k &= -2\left[1 + \epsilon(t) - \cos k\right] v_k - 2\epsilon(t) \sin k \; u_k \end{aligned} \tag{3.57}$$

We bring the above equation to standart Landau-Zener form by shifting time $\tau = t + \tau_Q(\cos k - 1)/(1 + \sin^2 k)$. Using convenient notation with Pauli matrices it reads:

$$i\frac{d}{d\tau} \begin{pmatrix} u_k^+ \\ u_k^- \end{pmatrix} = \left[\frac{\tau}{\hat{\tau}_Q}\, \sigma \;+\; \Delta'\, \sigma_\perp \right] \begin{pmatrix} u_k^+ \\ u_k^- \end{pmatrix} \;, \tag{3.58}$$

where $\sigma = (\sigma^x \sin k - \sigma^z)/\sqrt{1+\sin^2 k}$ and $\sigma_\perp = (\sigma^x + \sigma^z \sin k)/\sqrt{1+\sin^2 k}$ are two orthogonal spin components, $\hat{\tau}_Q = \tau_Q/2\sqrt{1+\sin^2 k}$ is the Landau-Zenner transition time, and $\Delta' = 2\sin k(1-\cos k)/\sqrt{1+\sin^2 k}$ is the minimal gap at the anticrossing center when $\tau = 0$.

In the slow transition limit, $\tau_Q \gg 1$, only the long wavelength modes $k \approx 0$ get excited and the probability of excitation is given by Landau-Zenner formula:

$$p_k \;=\; e^{-\pi\hat{\tau}_Q(\Delta')^2} \;\approx\; e^{-\pi\tau_Q k^6/2} \tag{3.59}$$

The density of quasiparticle excitations after crossing the multicritical point can be calculated as

$$d \;=\; \int_{-\pi}^{\pi} \frac{dk}{2\pi}\, p_k \;=\; d_0\, \tau_Q^{-1/6}\;, \tag{3.60}$$

where $d_0 = 2^{1/6}\Gamma(7/6)\pi^{-7/6} = 0.2394$ and Γ is the Gamma function.

As we have noticed in the Appendix A there is a problem here with defining critical exponents in an unambiguously way (A.19). The correct exponent 1/6 can be made compatible with the general Eq. (2.7) as follows. The instantaneous quasiparticle frequency in Eqs. (3.58) is $\omega'_k = \sqrt{(\epsilon')^2 + (\Delta')^2}$, where $\epsilon' = \tau/\hat{\tau}_Q$ is the relevant distance from the anticrossing center. We can expand $\omega'_k \sim |k|^3 \equiv |k|^{z'}$ at $\epsilon' = 0$ and small k. For small ϵ' $\omega'_0 \sim |\epsilon'| \equiv |\epsilon'|^{z'\nu'}$ and weidentify the exponents relevant for a homogeneous transition as

$$z' = 3\;,\quad \nu' = 1/3\;. \tag{3.61}$$

Using these relevant exponents in the general Eq. (2.7) gives the correct exponent 1/6 in the exact Eq. (3.60). Following [47] we can attribute this anomalous scaling and primed critical exponents to some quasicritical point which is located in ferromagnetic phase close to the multicritical point – which is in agreement with the interpretation that the critical point is effectively 'spread' over some distance in ferromagnetic phase.

We note here that both z in Eq. (A.19) and z' in Eq. (3.61) are greater than 1 so we can expect nontrivial dependence of critical $\hat{v}$ with α in inhomogeneous quench.

To close the discussion we can ask under which conditions can we have adiabatic evolution during homogeneous quench. Since a finite chain of N spins has finite energy gap at the critical $\epsilon = 0$, the homogeneous transition becomes adiabatic above a finite τ_Q when the scaling relation (3.60) crosses over to exponential decay.

Indeed, in a periodic chain the quasimomenta are quantized as $k = \pm\frac{\pi}{N}, \pm\frac{3\pi}{N}, ...$ to satisfy anti-periodic boundary conditions for the Jordan-Wigner fermions in the subspace of even parity. When τ_Q is large enough, then only the longest wavelength pair $\left(\frac{\pi}{N}, -\frac{\pi}{N}\right)$ has non-negligible excitation probability (3.59) $p_{\pi/N} = \exp\left(-\pi^7\tau_Q/2N^6\right)$, but even this probability becomes exponentially small when τ_Q is deep enough in the adiabatic regime:

$$\tau_Q \;\gg\; \frac{2}{\pi^7}\, N^6\;. \tag{3.62}$$

The transition time required for a homogeneous transition to become adiabatic grows with the sixth power of the number of spins.

3.4.2 Inhomogeneus static solution

Now we again turn our attention to general inhomogeneous situation with the Hamiltonian 3.52. This quadratic Hamiltonian is diagonalized to

$$H = \sum_m \omega_m \gamma_m^\dagger \gamma_m + \text{const} \tag{3.63}$$

by a (2Nx2N) Bogoliubov transformation (3.16) satisfying stationary Bogoliubov-de Gennes equations,

$$\omega u_n^\pm = 2(1+\epsilon_n) u_n^\mp (1 \mp \epsilon_{n+\frac{1}{2}}) u_{n+1}^\mp - (1 \pm \epsilon_{n+\frac{1}{2}}) u_{n-1}^\mp, \tag{3.64}$$

with $\omega \geq 0$ and $u_{m,n}^\pm \equiv u_{m,n} \pm v_{m,n}$.

We take the size of an open chain $N \to \infty$ to avoid boundary effects and consider a smooth static slant (3.26):

$$\epsilon_n \;=\; \tanh\left[\alpha(n-n_c)\right] \;\approx\; \alpha(n-n_c)\;, \tag{3.65}$$

interpolating between paramagnetic $\epsilon = 1$ and ferromagnetic $\epsilon = -1$, which is shown in Fig. 3.1. The slant (3.65) can be linearized near the critical point n_c as in the general Eq. (3.6).

We are interested in the low frequency part of the quasiparticle spectrum where, presumably, we can make a long wavelength approximation and treat n as a continuous variable:

$$u_{n\pm1} \approx u_n \pm \frac{d}{dn} u_n + \frac{1}{2}\frac{d^2}{dn^2} u_n\;. \tag{3.66}$$

We also expect that the low frequency quasiparticle modes are localized near the critical point n_c, where we can use the linearization in Eq. (3.65).

First we rescale energy scale and position as

$$x = \alpha^{1/3}(n-n_c)\;\;,\;\;\; \Omega = \alpha^{-3/4}\omega \tag{3.67}$$

and equations (3.64) can be rewritten as

$$\alpha^{\frac{1}{12}}\Omega \begin{pmatrix} u^+ \\ u^- \end{pmatrix} - \sigma^x \left[-\frac{d^2}{dx^2} + 2x\right] \begin{pmatrix} u^+ \\ u^- \end{pmatrix} \;=\; \alpha^{1/3}\; i\sigma^y \left[1 + 2x\frac{d}{dx}\right] \begin{pmatrix} u^+ \\ u^- \end{pmatrix}. \tag{3.68}$$

To leading order in $\alpha \ll 1$ their two eigenmodes of lowest frequency are

$$\begin{aligned} \Omega_0 \;&=\; 0\;, \\ u_0^+ \;&\propto\; e^{-\frac{1}{2}\alpha^{1/3}x^2} A(x)\;,\;\;\; u_0^- \propto 0\;, \end{aligned} \tag{3.69}$$

and

$$\begin{aligned} \Omega_1 \;&=\; \sqrt{8\Gamma(5/4)/\Gamma(3/4)} \;=\; 2.43\;, \\ u_1^+ \;&\propto\; e^{-\frac{1}{2}\alpha^{1/3}x^2} \frac{dA}{dx}(x)\;,\;\;\; u_1^- \propto e^{-\frac{1}{2}\alpha^{1/3}x^2} \frac{-2A(x)}{\alpha^{\frac{1}{12}}\Omega_1}\;, \end{aligned} \tag{3.70}$$

where $A(x) = \text{Ai}[2^{1/2}x]$ and Ai is the Airy function satisfying differential equation

$$\left[\frac{d^2}{dx^2} - x\right] Ai(x) = 0. \tag{3.71}$$

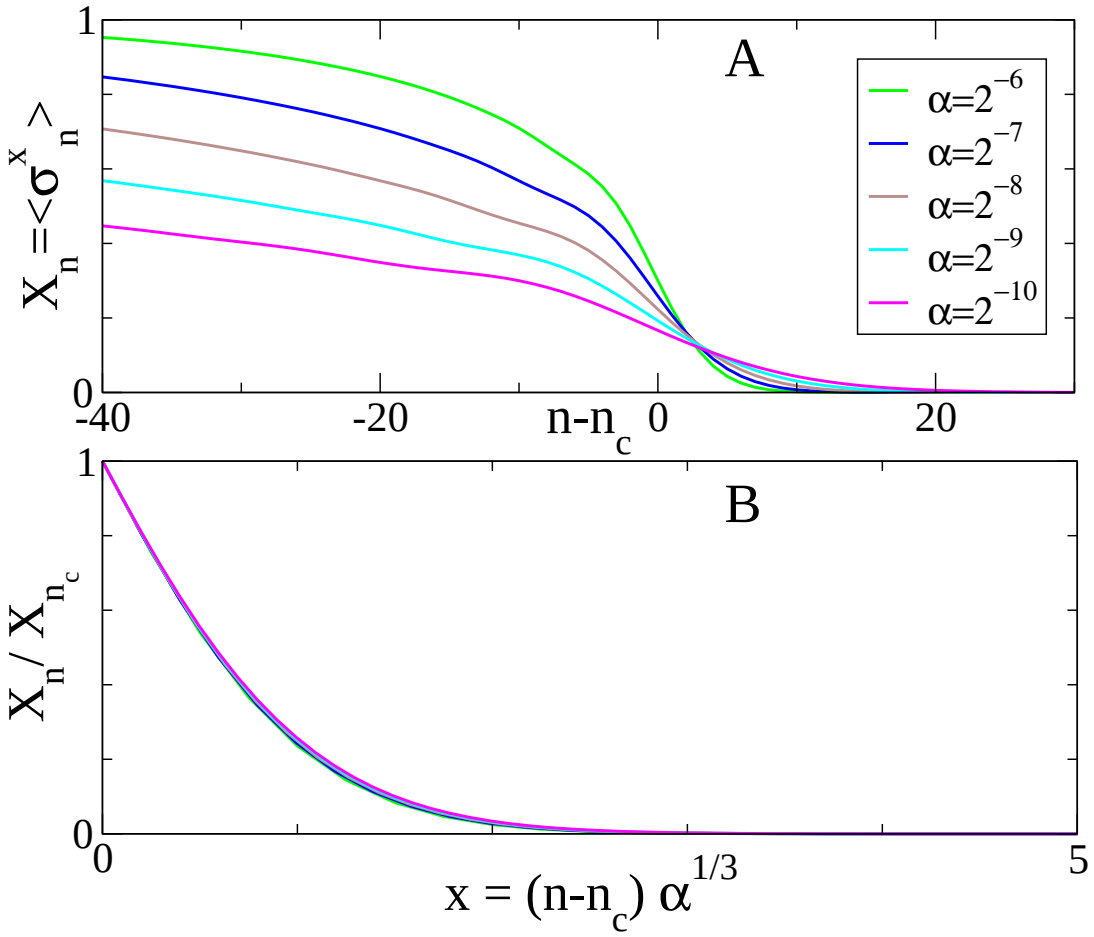

Figure 3.8: Phase transition in space. In A and B, exact numerical spontaneous ferromagnetic magnetization as a function of $n - n_c$ and $x = \alpha^{1/3}(n - n_c)$ in Eqs. (3.67) respectively. The spontaneous magnetization penetrates into the paramagnetic phase to a depth of $\delta x \simeq 1$, see B, i.e. $\delta n \simeq \alpha^{-1/3}$ in agreement with (3.73).

We can calculate the relevant excitation gap (even parity of excited quasipartices) as

$$\hat{\Delta} \;=\; \omega_0 + \omega_1 \;=\; \alpha^{3/4}\Omega_1 \;\simeq\; \alpha^{3/4}\;, \tag{3.72}$$

in agreement with the general Eq. (3.11) when we choose $z' = 1/\nu' = 3$ relevant for the homogenous transition (3.61).

On the other hand, the modes (3.69,3.70) do not have a unique scale of length. They penetrate into the paramagnetic phase, where $x > 0$, to a depth

$$\delta n \;\simeq\; \alpha^{-1/3} \tag{3.73}$$

determined by the $x \to +\infty$ asymptote of the Airy function $A(x) \sim \exp(-2\sqrt{2}x^{3/2}/3)$ and Eq. (3.67) and δn is consequently penetration depth of ferromagnetic magnetization into the paramagnetic phase. We illustrate this in Fig. 3.8, where we present numerical results obtained for the slant (3.65) in Fig. 3.1. This is consistent with general equation (3.10) when we take 'static' $\nu = 1/2$ in the paramagnetic phase in Eqs. (A.19). On the ferromagnetic side, where $x < 0$, the same modes (3.69,3.70) extend to the depth

$$\Delta n \;\simeq\; \alpha^{-1/2} \tag{3.74}$$

limited by the Gaussian envelope $e^{-\frac{1}{2}\alpha(n-n_c)^2}$. This envelope is damping oscillations of the Airy function $A(x)$ which take place on the shorter scale $\delta n \simeq \alpha^{-1/3}$. An overall width of the modes (3.69,3.70) is set by this longer scale Δn.

3.4.3 Inhomogenouse quench - large velocity limit

The time-dependent equivalent of static (3.64) Bogoliubov- de Gennes equation reads:

$$i\frac{d}{dt}u_n^{\pm} = 2(1+\epsilon_n)u_n^{\mp} - (1\mp\epsilon_{n+\frac{1}{2}})u_{n+1}^{\mp} - (1\pm\epsilon_{n+\frac{1}{2}})u_{n-1}^{\mp} \ . \tag{3.75}$$

We solve that equation numerically and the results for number of kinks in large velocity limit are presented below.

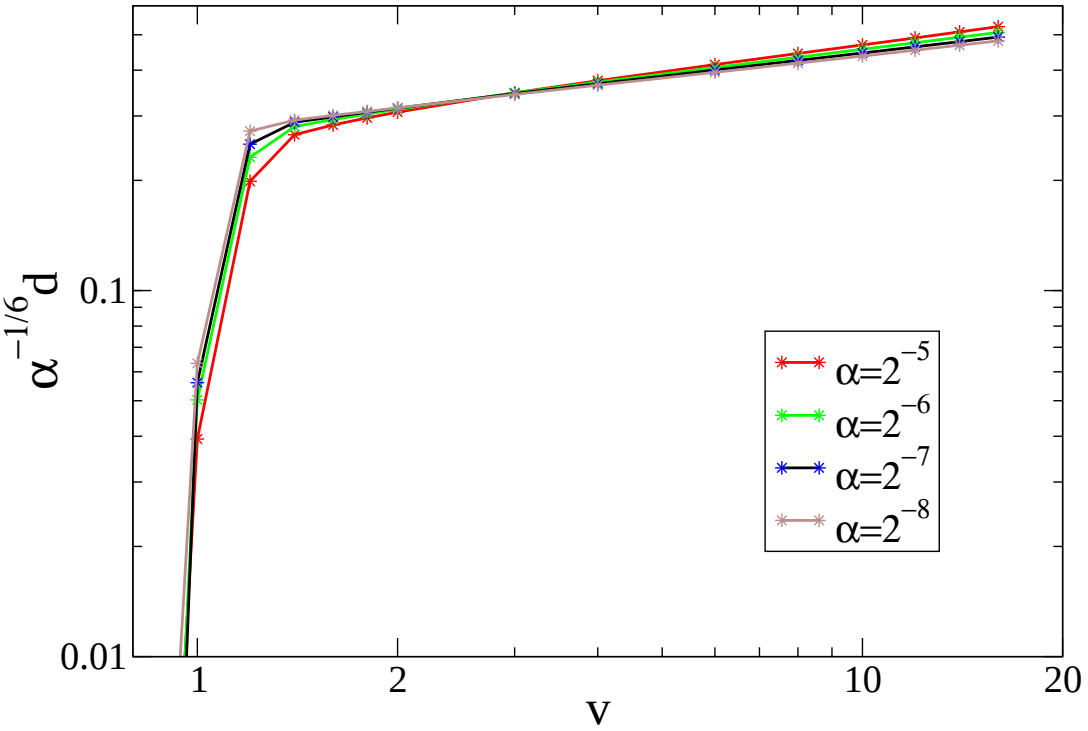

Figure 3.9: Numerical simulations of the time-dependent Bogoliubov-de Gennes equations (3.75) in a finite chain of $N = 200$ spins. Log-log plot of rescaled final kink density $\alpha^{-1/6}d$ after an inhomogeneous transition in Eq. (3.28) for different degrees of inhomogeneity α. In the homogeneous regime – which we safely attribute here to $v \gg 2$ – the plots nearly collapse and almost linear with a slope 0.20 for $\alpha = 1/256$. This is close to the predicted 1/6 in Eq. (3.76) where $\alpha^{-1/6}d \simeq v^{1/6}$.

We are not able to give any analytical prediction in the long wavelength version of Eq. (3.75). This can be attributed to nontrivial value of z exponent which results in higher order differential equation in t after we move to reference frame co-moving with the front – like in (3.33) – or 'homogenouse' one – like in (3.37).

We can obtain quasiparticle group velocity at the critical point $\epsilon = 0$ from the dispersion (A.12). The group velocity is maximized for $k = \pm\pi/2$ by $v_q = 2$ .When $v \gg v_q$ there is no causal connection across the critical point and the inhomogeneous transition

should proceeds as if it were effectively homogeneous with a quench time $\tau_Q = 1/\alpha v$. In this regime we expect the "homogeneous" 1/6-scaling in Eq. (3.60) to apply and a rescaled final density of kinks to scale as

$$\alpha^{-1/6}\, d \;\simeq\; v^{1/6} \tag{3.76}$$

with velocity of the critical front v. The numerical results are shown in Fig. 3.9 and in the homogeneous regime $v \gg 2$ they are consistent with the prediction (3.76), but numerical simulation are not enough pinpoint where 'homogenouse regime' breaks. In particularly, when we might expect some dependence on α and possible nontrivial 'relativistic' correction from finite v like for the Ising model (3.44).

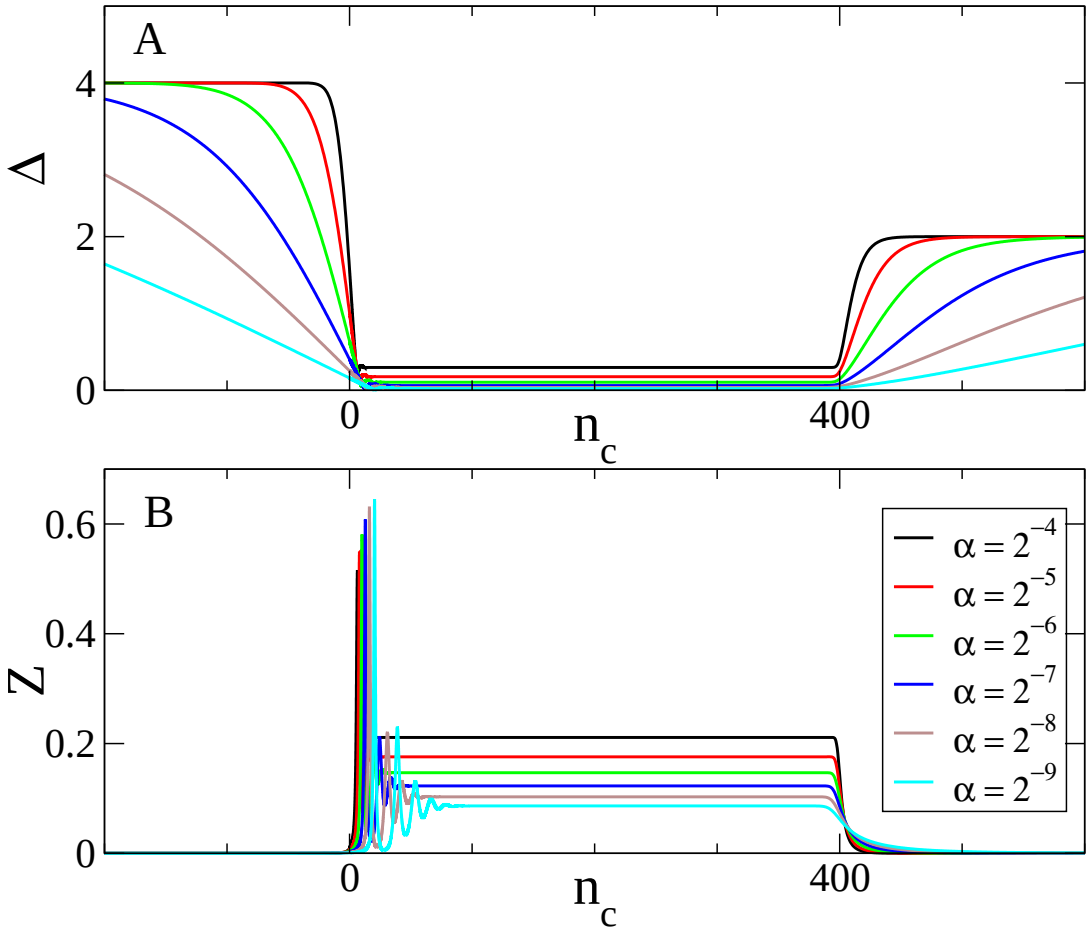

Figure 3.10: Parameters Δ and Z in Landau-Zener equation (3.47) calculated numerically as a function of n_c for several values of gradients α in (3.65). Size of the system $N = 400$.

3.4.4 Inhomogenouse quench - small velocity limit

We proceed in the analogous way as for the Ising model. We assume that for small enough velocity only the lowest excited state can get populated during the evolution. . Due to conserved parity it is a state occupied by two lowest quasiparticles γ_0 and γ_1 and

we truncate the Hilbert space to the ground state and that state:

$$|\psi(t)\rangle \;=\; a(t)\;|0\rangle \;+\; b(t)\;|1\rangle\;, \tag{3.77}$$

where $|0\rangle$ is the instantaneous ground state and $|1\rangle = \gamma_1\gamma_0|0\rangle$. The amplitudes (a,b) solve a generalized Landau-Zener problem (3.47), with the initial conditions $(a(-\infty), b(-\infty)) = (1, 0)$. The instantaneous gap $\Delta = \omega_0 + \omega_1$ and overlap change Z (3.48) for the model are presented in Fig. 3.10 A and B respectively. In the bulk, when $1 \ll n_c \ll N$ the value of the gap Δ is calculated in Eqs. 3.72 and scales as $\sim \alpha^{3/4}$. The bulk value of Z can be estimated from Eqs. (3.48, 3.69, 3.70) and scales as $\sim \alpha^{1/4}$. We solve the Landau-Zener problem (3.47) numerically:

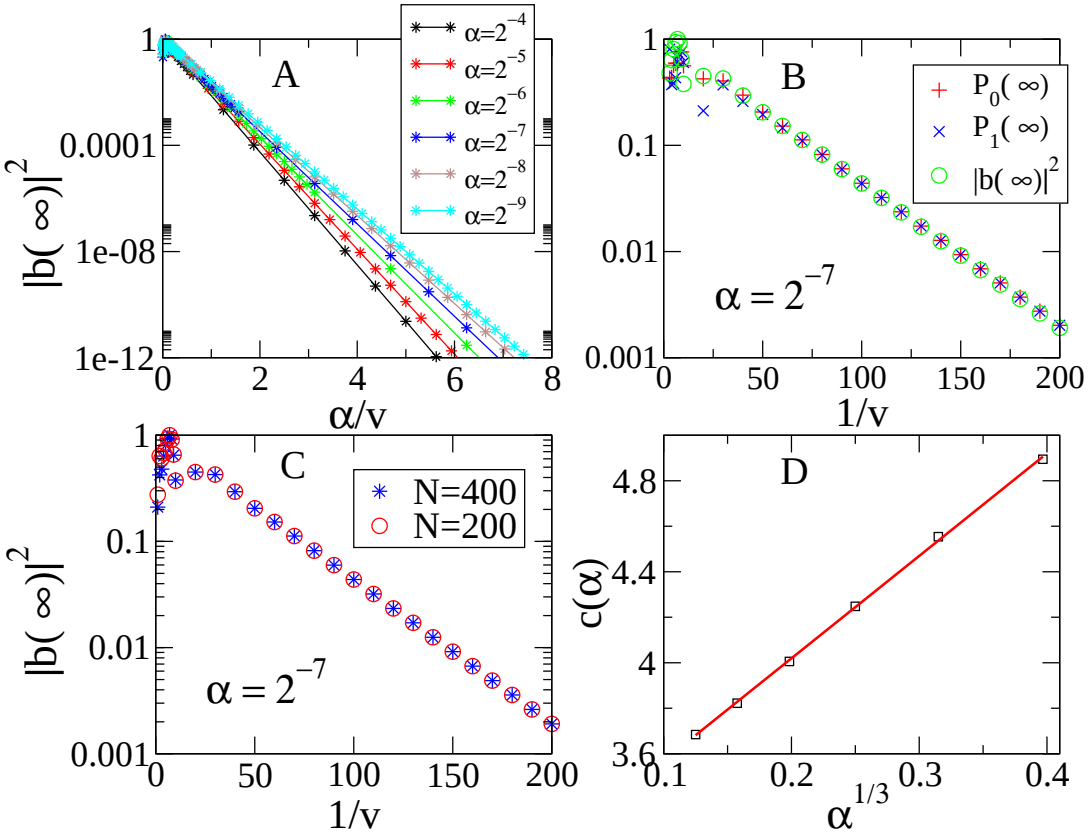

Figure 3.11: In panel **A**, the final excitation probability $|b(\infty)|^2$ in the generalized Landau-Zener problem, defined in Eq. (3.47) and Fig. 3.10, as a function of α/v for different values of the inhomogeneity α. In panel **B**, $|b(\infty)|^2$ from the Landau-Zener model and corresponding excitation probabilities $P_0 = \langle\gamma_0^\dagger\gamma_0\rangle$ and $P_1 = \langle\gamma_1^\dagger\gamma_1\rangle$ from the exact Bogoliubov-de Gennes equations (3.75). In panel **C**, $|b(\infty)|^2$ as a function of $1/v$ for a fixed $\alpha = 2^{-7}$ and two different chain sizes $N = 200, 400$. For small v the excitation probability does not depend on N demonstrating that the excitation of the lowest two quasiparticles is a boundary effect. In panel **D**, the coefficients c fitted from panel A as a function of α. The solid line is the best fit $c = 3.12 + 4.50\alpha^{1/3}$ demonstrating weak residual dependence on $\alpha^{1/3}$ which becomes negligible when $\alpha \to 0$ and $c \to 3.12$.

Numerical probability of excitation of the Landau-Zenner equation (3.47) is well described by a simple Landau-Zener -like formula

$$|b(\infty)|^2 \;=\; \exp\left(-c\,\frac{\alpha}{v}\right)\;, \tag{3.78}$$

Here $c = O(1)$ is a numerical pre-factor. Indeed, the plots for different α (see Fig. 3.11 A) nearly collapse. The collapse is not perfect because, as shown in Fig. 3.11 D, there is a weak residual dependence $c \approx 3.12 + 4.50\ \alpha^{1/3}$. However, when $\alpha \to 1$ then $c \approx 3.12$ becomes independent of α as assumed in Eq. (3.78).

Fig. 3.11 B, where we compare Landau-Zener simulation with the results for full Bogoliubov-de Gennes equation (3.75), confirms our assumption that only the lowest pair of quasiparticles gets excited. Probability of excitation of next quasiparticle - not shown on the plot - is exponentially smaller.

Furthermore, Fig. 3.11 C shows that in the adiabatic regime the small excitation probability $|b(\infty)|^2$ does not depend on the chain size N. Not quite surprisingly, the excitation of the lowest two quasiparticles is a boundary effect determined by the behavior of Δ and Z in Fig. 3.10 when the critical point n_c is near the ends of the chain.

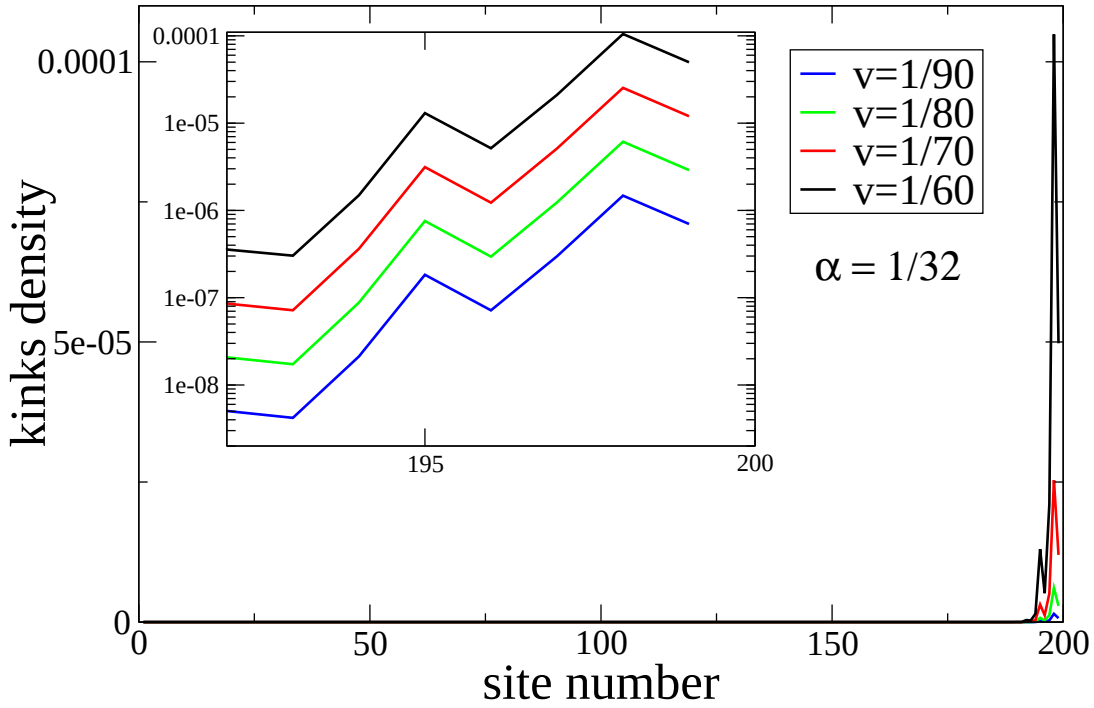

Figure 3.12: Density distributions of kinks along a chain of $N = 200$ spins after an inhomogeneous transition in the adiabatic regime $v \ll \alpha$. These distributions were obtained from numerical simulations of the exact time-dependent Bogoliubov-de Gennes equations (3.75) with the critical front in Fig. 3.1. Residual (exponentially small) excitations are brushed away by the critical front to the right edge leaving behind defect-free bulk of the chain. The inset is a log-scale focus on the right edge. It shows that in the adiabatic regime all density distributions for different v are the same up to an overall v-dependent amplitude set by the Landau-Zener excitation probability in Eq. (3.78).

Taking those results into account we see that the excitation probability (3.78) is exponentially small when $v \ll \alpha$. This allows us to identifies a threshold velocity

$$\hat{v} \simeq \alpha \tag{3.79}$$

when the inhomogeneous transition becomes adiabatic. As anticipated for $z > 1$ – see (3.12) – the adiabatic threshold $\hat{v}$ is a positive power of the gradient α. However, due to the problems with unambiguously defining critical exponent we are not able to check the exact scaling in (3.12).

Identically as for the Ising model, we can expect that these exponentially small excitation should be brushed to the end of the chain by a critical front – and they are leftover of the critical front leaving the chain. This is confirmed in Fig. 3.12 where we simulate numerically full Bogoliubov-de Gennes equation (3.75) for several small velocities and look at excited kinks.

3.5 Conclusion

Concluding what we have learned in this chapter we should stress that smooth inhomogeneity results in a small energy gap and that allows us to avoid exciting the system when the critical front is moving slow enough. That is why the time necessary to prepare the final state in an adiabatic way scales as $N/\hat{v}$. Critical velocity here $\hat{v}$ – in principle – depends on α but as we have seen do not have to be extremely small and do not depend on N.

On the other hand when we cross the critical point in an homogeneous way we can expect the small energy gap resulting from Finite Size Effects which scales at the critical point as $N^{-}z$. This can result in an adiabatic transition but as have seen the transition time scales here like $N^{\frac{z\nu+1}{\nu}}$. For the Ising model the time necessary for adiabatic quench is (2.24) N^2 and for the XY multicritical point (3.62) N^6.

Putting the results together, we can conclude that for large N an inhomogeneous transition is a more efficient method of adiabatic quantum state preparation than a straightforward homogeneous transition. Not only the time required for an adiabatic transition is much shorter, but also any residual excitations are brushed away to the end of the spin chain. This may be of relevance for an adiabatic state preparation in quantum simulators mentioned in the Introduction.

Chapter 4

Quench with decoherence

In the previous chapters we have studied quench dynamics in isolated systems. Now we will bring our attentions to dynamical transition in open quantum systems. Motivation for such studies come, for example, from condensed matter physics. Contrary to cold atoms in optical lattice it is almost impossible here to isolate the system from its environment, which – as we will see - might have a profound effect on the results of the transition.

In general, the problem is considerably harder then for closed systems and still a lot of work is necessary to understand it better. Most of the progress has been achieved studying quantum Ising chain. Ref. [48, 49] considered 'global' case when all spins were coupled to (the same) hermitian operator of the environment. This global model is solvable thanks to its translational invariance – and its solution indicates that decoherence is increasing density of excited quasiparticles as compared to an isolated system. A local model, where the Ising model coupled to an Ohmic heat bath, was analyzed in Ref. [50] distinguishing between different regimes of parameters where defect production is dominated either by Kibble-Zurek Mechanism or external heating.

In this chapter, we are going to consider another – quite realistic –example of dynamical quench with decoherence. Namely we will focus on the Ising model coupled locally to a static spin environment. In this case the influence of the environment turn out to be dramatic making adiabatic transition exponentially harder.

Results presented in this chapter have been published in [II].

4.1 Ising chain in static spin bath

The Hamiltonian can be written in general form:

$$H = H_{sys} + H_{env} + H_{int} \tag{4.1}$$

where we have singled out parts of Hamiltonian for the system $\mathcal{S}$, environment $\mathcal{E}$ and interaction between the two respectively. H_{sys} is the familiar Ising model:

$$H \;=\; -\sum_{n=1}^{N} \left(\sigma_n^x \sigma_{n+1}^x + g(t)\sigma_n^z\right) \;. \tag{4.2}$$

with periodic boundary conditions and we quench external magnetic field $g(t) = -\frac{t}{\tau_Q}$ as in Chapter 2. The magnetic field is ramped down from paramagnetic $g = +\infty$ to

ferromagnetic $g = 0$ with the quench rate τ_Q. We couple the Ising chain (4.2) to an environment $\mathcal{E}$ of M spins through the interaction

$$H_{int} \;=\; -\sum_{n=1}^{N}\sum_{m=1}^{M} \sigma_n^z \; V_{nm} \; \sigma_{\mathcal{E}m}^z \; . \tag{4.3}$$

Here $\sigma_{\mathcal{E}m}$ are Pauli matrices of environmental spins. We assume that he environment is static so that

$$H_{env} = 0 \tag{4.4}$$

Initially at $t \to -\infty$ the system is in the ground state $|g \to \infty\rangle$ of the pure Ising chain (4.2) with all spins polarized along z-axis and is uncorrected from the environment. This is a popular assumption is studies of decoherence, which while making the problem considerably easier is often not valid in the realistic situations. Here, however, this is perfectly reasonable because large initial energy gap of $2g$ makes the influence of the static environment so negligible that the initial states of the system S and environment E can be assumed uncorrelated: $\rho_{\mathcal{S}+\mathcal{E}} = \rho_{\mathcal{S}} \otimes \rho_{\mathcal{E}}$ with $\rho_S = |g \to \infty\rangle\langle g \to \infty|$ and the environment is initially in a pure state

$$\sum_{s_1,...,s_M=-1,+1} c_{s_1,...,s_M} \; |s_1\rangle ... |s_M\rangle \; . \tag{4.5}$$

Here $\sigma_{\mathcal{E}m}^z |s_m\rangle = s_m |s_m\rangle$ is written in σ_z base.

After evolution for some time Δt the reduced density matrix of the system

$$\rho_{\mathcal{S}} = \mathrm{Tr}_{\mathcal{E}} \; \rho_{\mathcal{S}+\mathcal{E}} \tag{4.6}$$

takes the form

$$\begin{aligned} \rho_S(\Delta t) \;&=\; \sum_{\vec{s}} |c_{\vec{s}}|^2 \; U(\Delta t, \vec{s}) \; |0_\infty\rangle\langle 0_\infty| \; U^\dagger(\Delta t, \vec{s}) \\ &\equiv\; \overline{U(\Delta t, \vec{s}) \; |0_\infty\rangle\langle 0_\infty| \; U^\dagger(\Delta t, \vec{s})} \; . \end{aligned} \tag{4.7}$$

Here $\vec{s} = (s_1, ..., s_M)$ for simplicity,

$$U(\Delta t, \vec{s}) \;=\; \mathcal{T} \; \exp\left[-i \int_0^{\Delta t} dt' \; H(t', \vec{s}) \right] \; , \tag{4.8}$$

is unitary evolution operator for single z-configuration of the environment where effective Hamiltonian is

$$H(t, \vec{s}) \;=\; -\sum_{n=1}^{N} \left(\left[g(t) + \Gamma_n^{\vec{s}} \right] \; \sigma_n^z + \sigma_n^x \sigma_{n+1}^x \right) \tag{4.9}$$

with random magnetic fields resulting from interaction with the static environment

$$\Gamma_n^{\vec{s}} \;=\; \sum_{m=1}^{M} V_{nm} s_m \; . \tag{4.10}$$

The overline in Eq. (4.7) is an average over $\vec{s}$ with probability distribution $|c_{\vec{s}}|^2$, but it can also be interpreted as an average over random disorder field $\Gamma_n^{\vec{s}}$. $\rho_S(\Delta t)$ is an average over states $U(\Delta t, \vec{s})|0_\infty\rangle$ obtained in quenches with different disorder realizations for Hamiltonian (4.9). In this way, our original problem of a quench in the open pure Ising model (4.2) can be mapped to an average over quenches in the isolated random Ising model (4.9).

Here – in order to simplify the problem – we are going to assume that each spin of the environment couples to only one spin of the system or, in other words, each spin of the system has its own *local* environment. Consequently, Γ_m and Γ_n are statistically independent when $m \neq n$. We also assume that each Γ_n has the same Gaussian probability distribution

$$f(\Gamma) \;=\; \frac{e^{-\Gamma^2/2\sigma^2}}{\sqrt{2\pi\sigma^2}} \;, \tag{4.11}$$

where variance σ is strength of disorder/decoherence. This is a reasonable assumption when we assume that each local environment is large enough.

4.2 Random Ising model

The Hamiltonian (4.9) belongs to the universality class of the well known random quantum Ising chain. Full treatment of (static) model based on renormalization group technic can we found in [51] – see also references therein for earlier approaches. It has a continuous quantum critical point at g_c such that

$$\overline{\ln|g_c+\Gamma|} \;\equiv\; \int_{-\infty}^{\infty} d\Gamma\; f(\Gamma)\;\ln|g_c+\Gamma| \;=\; 0\;. \tag{4.12}$$

The phase diagram of the model is shown in Fig. 4.1.

There is no critical point for $\sigma > 1.887$ when the disorder is too strong. g_c separates ordered ferromagnetic phase from not-ordered paramagnetic phase. Besides there is a strip of Griffith's "phase" around g_c. No matter how weak σ is, the renormalization group transformation [51] drives the random Ising model (4.9) towards an infinite disorder fixed point with different critical exponents than in the pure Ising chain. In the random chain we have $\nu = 2$ and $z \to \infty$ instead $\nu, z = 1$ for pure case.

When we apply the standard Kibble-Zurek formula (2.7,2.6) for the exponent $\nu = 2$ and $z \to \infty$ we obtain domains size scaling like $\hat{\xi} \simeq 1$ and hence density of kinks $d \sim 1$. This results means that if there is a dependence of density of kinks d on the quench rate τ_Q it is weaker than (any) power low scaling.

In order to see that dependence we have to go back to the basic Kibble-Zurek argument in (2.3). It has been done in Ref. [52] where quench in random Ising model has been studied for the first time, see also [53] for more extended discussion. Following [51] the energy gap scales as $\Delta \sim \epsilon^{1/\epsilon}$, where ϵ marks distance from the critical point. Solving (2.3) in the leading order in τ_Q we obtain

$$\hat{\epsilon} \sim \ln^{-1}\tau_Q \tag{4.13}$$

and

$$\hat{\xi} \sim \ln^{2}\tau_Q \tag{4.14}$$

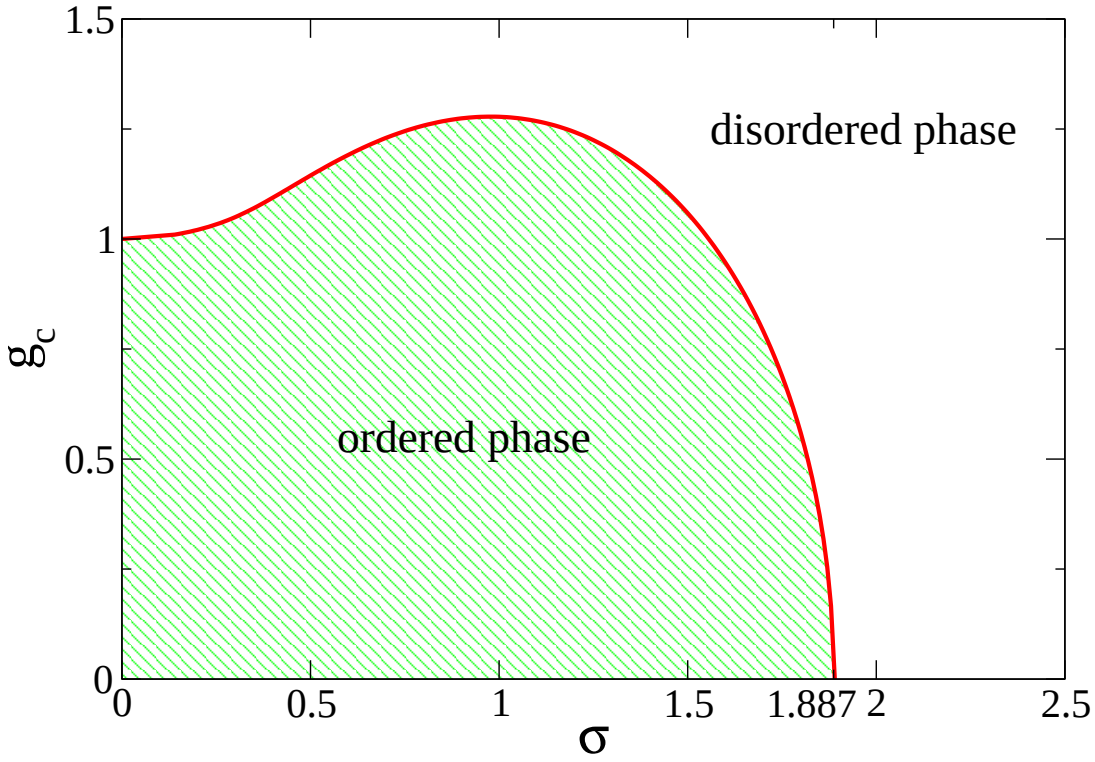

Figure 4.1: Schematic phase diagram for random Ising chain in (4.9) with disorder (4.11).

The estimate (4.14) was confirmed by numerical studies in Ref. [52, 53], where it was also noticed that for weak disorder and relatively fast quenches one recovers power-low dependence in eqs. (2.6,2.8) as in the pure case, see Eq. (4.2) and Chapter 2.

In the present model (4.9), it is relatively easy to estimate how slow a quench needs to be for the system to 'notice' the disorder and change its behavior from power-law scaling (2.6) to logarithmic (4.14). Assuming that influence of Γ_n is negligible, evolution becomes non-adiabatic at a distance from the critical point $\hat{\epsilon} \sim \tau_Q^{-1/2}$ (2.5). This assumption is not self-consistent when the remaining distance $\hat{\epsilon}$ is less than the strength σ of disorder field Γ_n, or equivalently

$$\tau_Q \, \sigma^2 \gg 1 \, . \tag{4.15}$$

Thus, no matter how weak the decoherence is, its influence is not negligible when the transition is slow enough: $\tau_Q \gg \sigma^{-2}$.

4.3 Density of kinks after the quench

In this section we present the results of numerical simulation for avarange density of kinks after the quench. As in the previous Chapters the Hamiltonian (4.9) is mapped via the Jordan-Wigner transformation (A.3) to free fermions system

$$H = \sum_{n=1}^{N} \left[g(t) + \Gamma_n \right] \left(2c_n^\dagger c_n - 1 \right) - \sum_{n=1}^{N} \left(c_n^\dagger c_{n+1} + c_{n+1} c_n + \text{h.c.} \right) , \tag{4.16}$$

with anti-periodic boundary condition (even parity). The model is solved using time-dependent Bogoliubov-de Gennes method in Heisenber picture where the state remains a vacuum for quasiparticle operators

$$\tilde{\gamma}_m = u^*_{nm}(t)c_n + v^*_{nm}(t)c^\dagger_n \ , \\ \tilde{\gamma}^\dagger_m = u_{nm}(t)c^\dagger_n + v_{nm}(t)c_n \ . \tag{4.17}$$

with the Bogoliubov modes $u_{nm}(t)$ and $v_{nm}(t)$ solving time-dependent Bogoliubov-de Gennes equations

$$i\frac{du^\pm_{n,m}}{dt} = 2\left[g(t) + \Gamma_n\right] u^\mp_{n,m} - 2u^\mp_{n-1,m} \ , \tag{4.18}$$

for details see Sec. 2.2. In order to quantify how much the system got excited we look at density of kinks after the transition. The final density of kinks at $g = 0$ is shown on a log-log plot in Fig. 4.2.

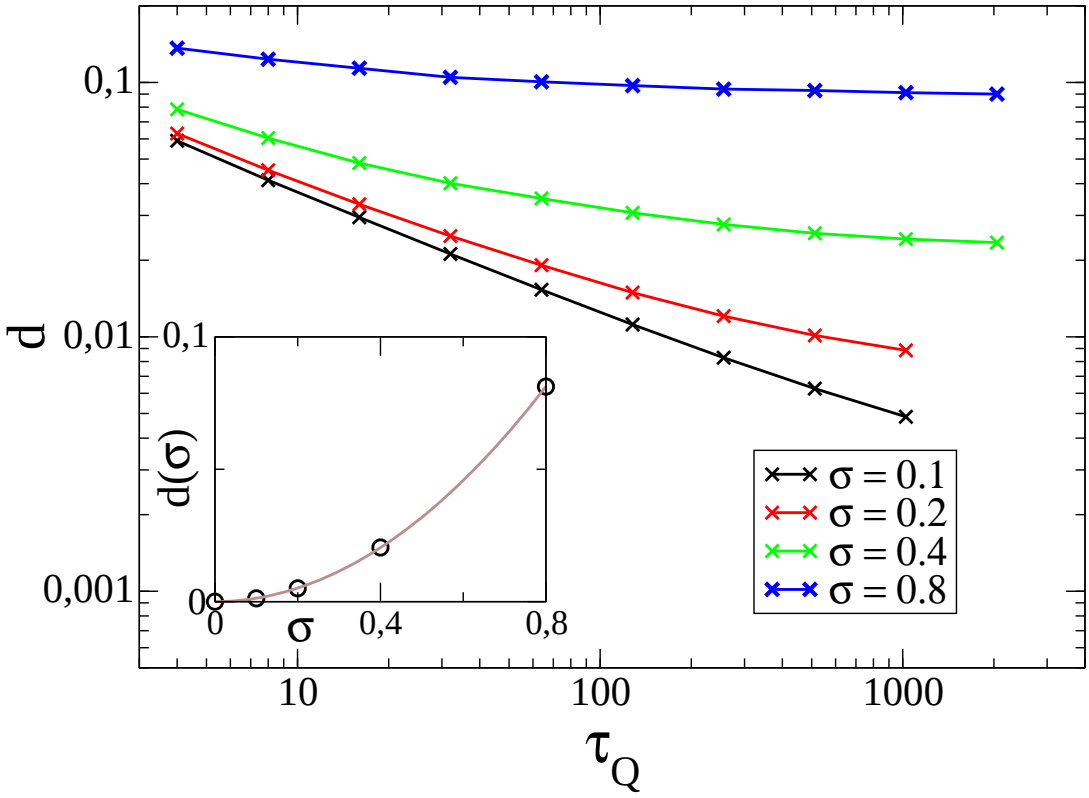

Figure 4.2: Density of kinks after the quench at final g=0 as a function of transition rate τ_Q for several values of disorder strength σ. The results here are obtained for a chain size N=512. For large τ_Q density of kinks tends to saturate on a 'static' value $d(\sigma)$. It has been shown in the inset where straight line $\frac{1}{8}\sigma^2$ can be easily obtained from perturbation expansion in small σ.

For large τ_Q, the density tends to saturate at non-zero $d(\sigma)$ shown in the inset in Fig. 4.2. $d(\sigma)$ is a static number of kinks emerging when we apply random magnetic field Γ_n

in (4.9) to the pure Ising model (4.2) for $g = 0$. It can be found analytically for small disorder σ by perturbation expansion $d(\sigma) \simeq \frac{1}{8}\sigma^2$.

In Fig. 4.3 we show a log-log plot displaying a difference $\delta d = d - d(\sigma)$ which can be attributed to the non-adiabaticity of the transition described by Kibble-Zurek Mechanism. If $\delta d = \alpha \tau_Q^w$, then in the log-log plot of Fig. 4.3 we would see a line $\log_{10} \delta d = \log_{10} \alpha + w(\log_{10} \tau_Q)$, but this is not the case when $\tau_Q \gg \sigma^{-2}$. At best we can think of a local slope $w(\tau_Q)$ which can be estimated by fitting to pairs of nearest neighbor data points. For weak σ and small τ_Q the slope w is close to the $-1/2$ characteristic for the pure model (4.2): fast quenches, when $\tau_Q \ll \sigma^{-2}$, become non-adiabatic far enough from the critical point not to see any effect of weak disorder. At stronger σ or longer τ_Q the local slopes are less steep and for a fixed σ they become less steep with increasing τ_Q. For example, at the strongest $\sigma = 0.8$ the local slope falls to a mere $|w| = 0.04$ for the longest τ_Q. These observations are consistent with the predicted logarithmic dependence of the dynamical correlation length $\hat{\xi}$ in Eq. (4.14).

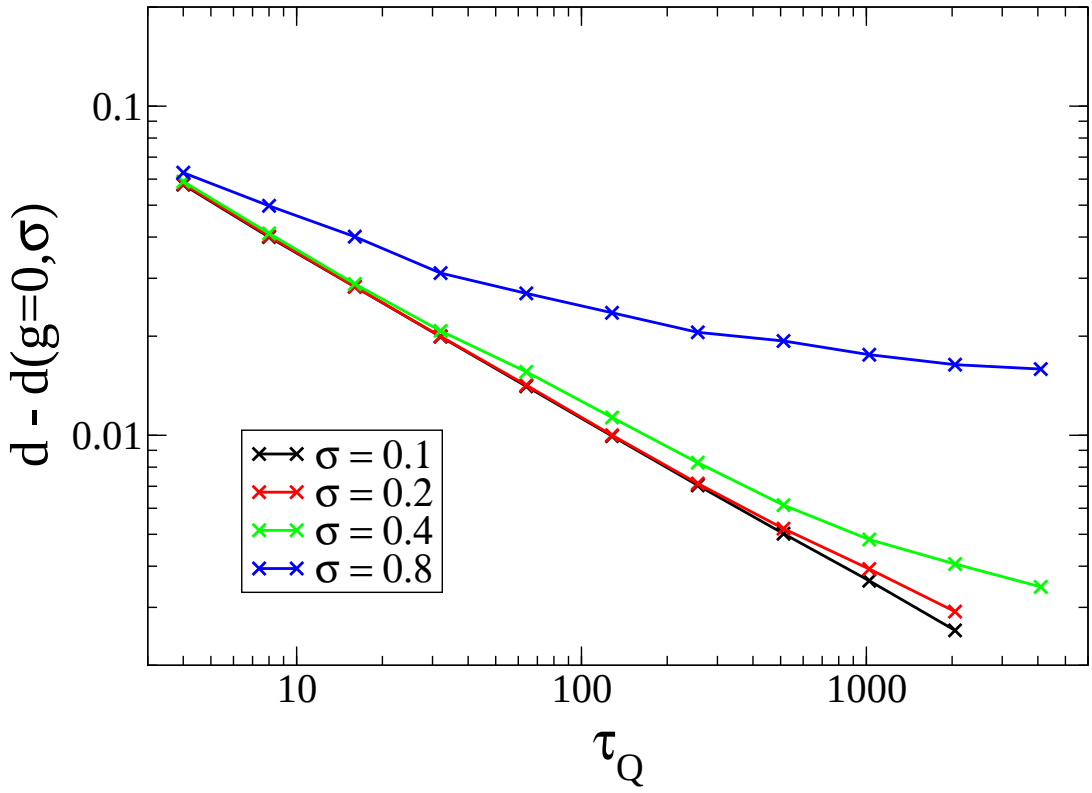

Figure 4.3: Difference $\delta d = d - d(\sigma)$ equal the density of kinks obtained above the ground state of random Ising model. Subtraction from data in Fig. 4.2. Size of the system N=512.

4.4 Conclusion

In this chapter we have seen that interaction with the environment can indeed have a profound effect on the result of the quench. When the system – Ising model – is isolated

from th environment, then (2.24) implies that the minimal evolution time τ_Q required to keep the evolution adiabatic (equivalently, to make $\hat{\xi} \gg N$) is

$$\tau_Q^{\text{isolated}} \simeq N^2 . \tag{4.19}$$

which is polynomial in N. In contrast, in our model of decoherence similar argument predicts

$$\tau_Q^{\text{open}} \simeq e^{\sqrt{N}} \tag{4.20}$$

for larger τ_Q (weeker disorder σ) which is non-polynomial in N. The maximal size of the system with no kinks is further limited by static influence of random magnetic field $d(\sigma)$ as shown in inset of Fig. 4.2. It sets the upper bound on the system size which for wear decoherence scales as σ^{-2}.

Chapter 5

Conclusion

Summarizing, lets review the most important findings described in this thesis. The thesis focuses on description of quench dynamics across quantum critical points and – I believe – we were able to obtain quality picture of the process. The results support and extend universal Kibble-Zurek mechanism, the theory which describes and predicts – among, many others – formation of topological defects resulting from crossing critical point at a finite rate.

Firstly, we study the properties of the state of the system following the quench. By looking at fidelity we are able to further support the picture coming from adiabatic-impulse approximation, which stands at the cornerstone of Kibble-Zurek mechanism. We investigate correlation functions both during the quench and after the quench. While correlation functions are mostly governed by dynamical Kibble-Zurek correlation length $\hat{\xi}$ we recognize that evolution of excited (after the transition) state results in additional non-universal characteristics of the state. We should keep in mind that Ising model if effectively a free fermion theory and we do not expect various collisions/relaxation processes between excited quasiparticles. Despite this simplicity we are still able to observe the effect of dephasing of the system. It appears through the development of other characteristic scale of length l. We should mention that in general system relaxation processes should be more prominent, at least on long enough scales of time. All obtained universal power-law scaling are in agreement with theoretical predictions.

Secondly, we develop the theory describing quench dynamics in spatially inhomogeneous (but still smooth) systems. We predict that when the quench is slow enough we can expect dramatic suppression in number of excited defects. We test these predictions in both Ising model and XY multicritical point and the results are consistent with theoretical predictions. Those results might sound like a negative results from the point of view of testing Kibble-Zurek theory. However, from the point of view of adiabatic quantum computation or adiabatic quantum state preparation it is the Kibble-Zurek mechanism itself that is a negative result: no matter how slow the homogeneous transition is there is a finite density of excitations which decay as a fractional power of transition rate τ_Q . From this perspective, the inhomogeneous transition may be a practical way to suppress Kibble-Zurek excitations and prepare the desired final ground state in an adiabatic manner.

Finally, we bring our attention to quench dynamics in open quantum system. We study the quantum Ising model coupled locally to static spin bath. From the point of view

of adiabatic state preparation the results indicate the possibility of crossing the critical point without exciting the system is strongly limited. In our model the system, due to interaction with environment – effectively changes the universality class. This results in much weaker – logarithmic in place of power-law – dependence of topological defects on the quench rate. Besides there appears topological defects due to static interaction with environment further limiting the size of the system which we can prepare adiabatically.

While the analytical and numerical results presented in the thesis are derived for solvable 1D quantum Ising model and likewise, we conjecture that similar behavior will be encountered in other quantum phase transitions. Thereafter, their non-equilibrium evolution can be anticipated using equilibrium critical exponents via Kibble-Zurek mechanism. This conjecture can be then tested in a variety of systems that undergo quantum phase transitions both in condensed matter and in atomic physics experiments.

Appendix A

Solution of 1D Quantum XY model

In this section I will recall standard solution of the 1D quantum spin-1/2 XY model (see e.g. [2, 54]) setting notation and presenting some of the methods that are being used in the thesis.

Quantum XY chain is described by the Hamiltonian:

$$H = -\sum_{i=1}^{N} \left(\frac{1+\gamma}{2} \sigma_i^x \sigma_{i+1}^x + \frac{1-\gamma}{2} \sigma_i^y \sigma_{i+1}^y + g\sigma_i^z \right) \tag{A.1}$$

where we assume periodic bundary condition

$$\sigma_1 = \sigma_{N+1}$$

. Magnetic field g is pointing in z-direction. γ is parameter describing anisotropy of ferromagnetic spin-spin interaction on XY plane. We will be particularly interested in fully anisotropic case when $\gamma = 1$, namely quantum Ising model.

$$H = -\sum_{n=1}^{N} \left(\sigma_n^x \sigma_{n+1}^x + g\sigma_n^x \right) . \tag{A.2}$$

It is one of the paradigmatic models of the Quantum Phase Transition [2]. For simplicity – without loss off generality – we assume that the number of spins N is even.

We start the diagonalization of Hamiltonian with nonlocal Jordan-Wigner transformation [55] :

$$\begin{aligned} \sigma_n^x &= \left(c_n^\dagger + c_n \right) \prod_{m<n} (1 - 2c_m^\dagger c_m) , \\ \sigma_n^y &= i \left(c_n^\dagger - c_n \right) \prod_{m<n} (1 - 2c_m^\dagger c_m) , \\ \sigma_n^z &= 1 - 2c_n^\dagger c_n , \end{aligned} \tag{A.3}$$

where we introduce fermionic operators c_n satisfying anticommutation relations

$$\begin{aligned} \left\{ c_m, c_n^\dagger \right\} &= \delta_{mn}, \\ \{ c_m, c_n \} &= \left\{ c_m^\dagger, c_n^\dagger \right\} = 0. \end{aligned}$$

Following the transformation (A.3) the Hamiltonian (A.1) splits into two parts working respectively in subspaces with even and odd number of c-quasiparticle and takes the form

$$H \;=\; P^+\, H^+\, P^+ \;+\; P^-\, H^-\, P^- \;. \tag{A.4}$$

Above

$$P^\pm = \frac{1}{2}\left(1 \pm \prod_{n=1}^{N} \sigma_n^x\right) = \frac{1}{2}\left(1 \;\pm\; \prod_{n=1}^{N}\left(1 - 2c_n^\dagger c_n\right)\right) \tag{A.5}$$

are projectors on the subspaces with even (+) and odd (−) numbers of c-quasiparticles and

$$H^\pm = -\sum_n \left(\hat{c}_n^\dagger \hat{c}_{n+1} + \gamma\; \hat{c}_n^\dagger \hat{c}_{n+1}^\dagger - g\; \hat{c}_n^\dagger \hat{c}_n + \frac{g}{2} + \text{h.c.}\right), \tag{A.6}$$

are respective reduced Hamiltonians. The boundary conditions for the fermionic operators are: $\hat{c}_{N+1} = -\hat{c}_1$ for even (+) and $\hat{c}_{N+1} = \hat{c}_1$ odd (−) subspaces.

Since $[H, P^\pm] = 0$ the parity of the number of c-quasiparticles is a good quantum number. The ground state has even parity for any value of g and γ and so we can confine ourselves to the subspace of even parity here. We follow the diagonalization of H^+ with the Fourier transform:

$$c_n \;=\; \frac{e^{-i\pi/4}}{\sqrt{N}} \sum_k c_k e^{ikn} \;, \tag{A.7}$$

To make the Fourier transform consistent with the antiperiodic boundary condition $c_{N+1} = -c_1$ pseudomomenta k take values:

$$k \;=\; \pm\,\frac{1}{2}\frac{2\pi}{N},\;\; \pm\,\frac{3}{2}\frac{2\pi}{N}, \ldots, \pm\frac{N-1}{2}\frac{2\pi}{N} \;. \tag{A.8}$$

It transforms the Hamiltonian into

$$H^+ \;= \sum_k \left\{ 2[g - \cos(k)] c_k^\dagger c_k + \gamma \sin(k) \left[c_k^\dagger c_{-k}^\dagger + c_{-k} c_k\right] - g \right\} \;. \tag{A.9}$$

Diagonalization of H^+ is completed by the Bogoliubov - de Gennes transformation

$$\begin{aligned} c_k &= u_k \gamma_k + v_{-k}^* \gamma_{-k}^\dagger \;, \\ c_k^\dagger &= u_k^* \gamma_k^\dagger + v_{-k} \gamma_{-k} \;. \end{aligned} \tag{A.10}$$

where modes (u_k, v_k) can be found as the eigenstates of the stationary Bogoliubov-de Gennes equations

$$\begin{aligned} \omega\; u_k &= +2[g - \cos k]\; u_k + 2\gamma \sin k\; v_k \;, \\ \omega\; v_k &= -2[g - \cos k]\; v_k + 2\gamma \sin k\; u_k \;. \end{aligned} \tag{A.11}$$

There are two eigenstates for each k with eigenenergies $\omega = \pm\omega_k$, where

$$\omega_k \;=\; 2\sqrt{[g - \cos k]^2 + \gamma^2 \sin^2 k} \;. \tag{A.12}$$

The positive energy eigenstate ($\omega = +\omega_k$) can be conveniently written as:

$$(u_k, v_k) \;=\; [\cos(\theta_k/2), \sin(\theta_k/2)] \tag{A.13}$$

where the angle θ_k is given by

$$\tan(\theta_k) = \frac{\gamma \sin(k)}{g - \cos(k)}, \tag{A.14}$$

and defines the quasiparticle operator

$$\gamma_k \;=\; u_k^* c_k + v_{-k} c_{-k}^\dagger, \tag{A.15}$$

The negative energy eigenstate

$$(u_k^-, v_k^-) = (-v_k, u_k) \tag{A.16}$$

defines $\gamma_k^- = (u_k^-)^* c_k + v_{-k}^- c_{-k}^\dagger = -\gamma_{-k}^\dagger$. After the Bogoliubov transformation, the Hamiltonian takes the form:

$$H^+ \;=\; \sum_k \omega_k \left(\gamma_k^\dagger \gamma_k - \frac{1}{2}\right) \;. \tag{A.17}$$

This is a simple-looking sum of quasiparticles with half-integer pseudomomenta. However, thanks to the projection $P^+ \; H^+ \; P^+$ in Eq. (A.4) only states with even numbers of quasiparticles belong to the spectrum of H^+.

There are lines of critical point in the XY model and they can be identify by checking where the gap in the excitation spectrum closes. It is easy to check that the gap vanishes on the line $g = \pm 1$ for momentum $k_0 = 0$ ($g = 1$) and $k_0 = \pi$ ($g = -1$) and on the line $\gamma = 0$ and $-1 \leq g \leq 1$ formomentum $k_0 = \arccos(g)$. The critical line $g = \pm 1$ separates paramagnetic phase with $|g| > 1$, from the ferromagnetic phase with $|g| < 1$. In the ferromagnetic phase there is nonzero spontaneous magnetization in the direction of stronger anisotropy (x-direction for $\gamma > 0$ and y-direction for $\gamma < 0$). Moreover we can divide ferromagnetic phase on commensurate and incommensurate phase [54]. In the commensurate phase the minimal gap in ϵ_k is reached for momentum $k_0 = 0$ (for $g > 0$, when $g < 0$ $k_0 = \pi$). This happens when anisotropy is strong enough, namely $1 - \gamma^2 < |g|$. In the incommensurate state the minimal energy gap is reached for $k_0 = \arccos\left(\frac{g}{1-\gamma^2}\right)$ and this happens for weak anisotropy when $1 - \gamma^2 > |g|$.

We can extract many critical properties of the model by looking at energy gap (A.12). First we will analyze quantum Ising model (i.e. fixed maximal anisotroy $\gamma = 1$) and – too focus attention – we will concentrate on critical point with $g_c = 1$. In order to extract the correlation length critical exponent ν and dynamical critical exponent z it is enough to check how the gap vanishes at and near the critical point. When N is finite and we are at the critical point $g = g_c = 1$ we get from (A.12) $\Delta \sim 1/N$. Since for the finite system at the critical point Finite Size Scaling yield $\Delta \sim N^{-z}$ we get $z = 1$ for the Ising model. Similarly the gap close to critical point vanishes like $\Delta = |g - 1| = |g - g_c|^{z\nu}$ and we identify $\nu = 1$. Summing up in the for the Ising critical point the critical exponents are

$$z = 1, \;\; \nu = 1. \tag{A.18}$$

The second point we will be interested in is multicritical Lifshitz point for $\gamma_c = 0$ and $g_c = 1$. We will approach the critical point allong the line $(\gamma, g) = (-\epsilon, 1 + \epsilon)$ coming from paramagnetic phase for $\epsilon > 0$ to incommensurate ferromagnetic phase for $\epsilon < 0$ (with the

spontaneous magnetization in x-direction). We identify critical exponent z in the same way as for the Ising Model and at the critical point $\epsilon_c = 0$ the energy gap vanishes like $\Delta \sim 1/N^2 \sim N^{-z}$ giving $z = 2$. On the first sight $\omega_{k=0} \sim |\epsilon| \sim |\epsilon|^{z\nu}$ giving $\nu = 1/2$. On the other hand we enter incommensurate phase for $\epsilon < 0$ and we should be more careful. For negative ϵ we find $\Delta \sim |\epsilon|^{3/2}$ suggesting $\nu = 3/4$. In other words in this case we do not have one characteristic scale of length. Intuitively – because minimal energy gap for non-zero k is significantly shifted into ferromagnetic phase ($\epsilon_{min} \sim -k^2$) we can envision that the critical point is effectively 'spread' over some distance in ferromagnetic phase and that will strongly influence the results obtained for such transition. Summing up naively we could expect:

$$\begin{aligned} z = 2,\ \nu = \frac{1}{2},\ \text{for } \epsilon > 0, \\ z = 2,\ \nu = \frac{3}{4},\ \text{for } \epsilon < 0, \end{aligned} \tag{A.19}$$

but we have to be very careful here.

Appendix B

Landau-Zener equation and Weber functions

In this appendix we will concentrate on solving Landau-Zener equation (2.17) from Chapter 2.

$$\begin{aligned} i\frac{d}{d\tau}u_k &= -\frac{1}{2}(\tau\Delta_k)u_k + \frac{1}{2}v_k \ , \\ i\frac{d}{d\tau}v_k &= +\frac{1}{2}(\tau\Delta_k)v_k + \frac{1}{2}u_k \ , \end{aligned} \tag{B.1}$$

As derived in sec. 2.2, Δ_k is given by $\Delta_k^{-1} = 4\tau_Q \sin^2 k$. Time τ runs from $-\infty$ to $\tau_{\rm final} = 2\tau_Q \sin(2k)$ corresponding to $t_{final} = 0$. The solution of the Landau-Zener equations has a general form (see for example appendix in Ref. [30]):

$$\begin{aligned} v_k(\tau) &= -\left[aD_{-s-1}(-iz) + bD_{-s-1}(iz)\right] \ , \\ u_k(\tau) &= \left(-\Delta_k\tau + 2i\frac{\partial}{\partial\tau}\right)v_k(\tau) \ , \end{aligned} \tag{B.2}$$

with arbitrary complex parameters a, b which are fixed by initial condition i.e. $u_k(-\infty) = 1$ and $v_k(-\infty) = 0$. $D_m(x)$ is a Weber function, $s = \frac{1}{4i\Delta_k}$ and $z = \sqrt{\Delta_k}\tau e^{i\pi/4}$. The Weber function $D_\nu(z)$ is a solution of Weber differential equation:

$$\frac{d^2}{dz^2}D_\nu(z) + (\nu + \frac{1}{2} - \frac{1}{4}z^2)D_\nu(z) = 0. \tag{B.3}$$

The power series expansion of $D_\nu(z)$ is given by:

$$D_\nu(z) = 2^{\nu/2}\pi^{1/2}e^{z^2/4}\sum_0^\infty \frac{(-z\sqrt{2})^n}{n!\Gamma\left[\frac{1}{2}(1-n-\nu)\right]}. \tag{B.4}$$

We will be mostly interested in small k when z is large. The asymptotic of the Weber function in that case is

$$D_\nu(z) = z^\nu e^{-\frac{z^2}{4}}\left[\sum_{n=0}^N \frac{(-\frac{1}{2}\nu)_n(\frac{1}{2}-\frac{1}{2}\nu)_n}{n!(-\frac{1}{2}z^2)_n} + O(|z^2|^{-N-1})\right] \tag{B.5}$$

where $|arg(z)| < \frac{3}{4}\pi$, ν is fixed, $|z| \to \infty$ and $(a)_n = \Gamma(a+n)/\Gamma(a)$. To find asymtotic for other values of $\arg z$ we use connection formula:

$$D_\nu(z) \;=\; e^{i\pi\nu} D_\nu(-z) + \frac{\sqrt{2\pi}}{\Gamma(-\nu)} e^{i(\nu+1)\frac{\pi}{2}} D_{-\nu-1}(-iz) \tag{B.6}$$

Using the asymptotes of the Weber functions and given initial conditions when $\tau \to -\infty$ we get values of parameters

$$\begin{aligned} a &= 0 \\ |b|^2 &= \frac{e^{-\pi/8\Delta_k}}{4\Delta_k} \; . \end{aligned} \tag{B.7}$$

The solution of the linear quench problem simplifies then to:

$$\begin{aligned} v_k(\tau) &= -bD_{-s-1}(iz) \; , \\ u_k(\tau) &= \left(-\Delta_k \tau + 2i\frac{\partial}{\partial\tau}\right) v_k(\tau) \; . \end{aligned} \tag{B.8}$$

At the end of the quench for $t = 0$ and when $\tau = \tau_k = 2\tau_Q \sin(2k)$, the argument of the Weber function $iz = \sqrt{\Delta_k}\tau e^{i\pi/4} = 2\sqrt{\tau_Q} e^{i\pi/4} \cos(k)\mathrm{sign}(k)$. In the limit of large τ_Q the modulus of this argument is large for most k, except the neighborhoods of $k = \pm\frac{\pi}{2}$, and we can again use the asymptotes of the Weber functions. After some work we get the products

$$\begin{aligned} |u_k|^2 &= \frac{1-\cos k}{2} + e^{-2\pi\tau_Q \sin^2 k} \; , \\ |v_k|^2 &= 1 - |u_k|^2 \; , \\ u_k v_k^* &= \frac{1}{2}\sin k + \mathrm{sign}(k)\; e^{-\pi\tau_Q \sin^2 k} \sqrt{1 - e^{-2\pi\tau_Q \sin^2 k}}\; e^{i\varphi_k} \; , \\ \varphi_k &= \frac{\pi}{4} + \frac{\Delta_k \tau_k^2}{2} + \frac{\ln\Delta_k}{4\Delta_k} + \frac{\ln\tau_k}{2\Delta_k} - \arg\left[\Gamma\left(1 + \frac{i}{4\Delta_k}\right)\right] \; . \end{aligned} \tag{B.9}$$

Here $\Gamma(x)$ is the gamma function. We expect that for large τ_Q only modes with small $|k| \ll 1$ get excited. Parts $\frac{1-\cos k}{2}$ in $|u_k|^2$ and $\frac{1}{2}\sin k$ in $u_k v_k^*$ are the results of sewing excited modes for small k with static – nonexcited – modes for large k (see Appendix A).

In this long wave length limit, the products can be further simplified to

$$\begin{aligned} |u_k|^2 &= \frac{1-\cos k}{2} + e^{-2\pi\tau_Q k^2} \; , \\ |v_k|^2 &= 1 - |u_k|^2 \; , \\ u_k v_k^* &= \frac{1}{2}\sin k + \mathrm{sign}(k)\; e^{-\pi\tau_Q k^2} \sqrt{1 - e^{-2\pi\tau_Q k^2}}\; e^{i\varphi_k} \; , \\ \varphi_k &= \frac{\pi}{4} + 2\tau_Q - (2 - \ln 4)\tau_Q k^2 + k^2 \tau_Q \ln\tau_Q - \arg\left[\Gamma\left(1 + i\tau_Q k^2\right)\right] \; . \end{aligned} \tag{B.10}$$

which we have used in Eqs. (2.25).

Appendix C

Toeplitz matrix determinant

In this appendix we give a short 'dictionary' of methods used to calculate determinant of Toeplitz matrix which are necessary to calculate the ferromagnetic correlation function after transition in Eqs. (2.40). For extended discussion see for example [56] and references therein. Toeplitz matrix T is characterized by the condition $T_{m,n} = T_{m-n}$. We are interested in the determinant of $(n+1)x(n+1)$ matrix T.

$$D_n[f] \;=\; det(T_n) \;=\; det\left(\int_{-\pi}^{\pi} f(q)e^{-i(j-k)q}\frac{dq}{2\pi}\right)_{j,k=0}^{n} \tag{C.1}$$

$f(q)$ is called the generating function for Toeplitz matrix T_n. $f(q)$ is complex and periodic function of q i.e. $f(q) = f(q+2\pi)$.
We will concentrate generating functions with zero winding number:

$$\int_{-\pi}^{\pi}\frac{dq}{2\pi}\frac{d}{dq}log\ f(q) = 0 \tag{C.2}$$

When $f(q)$ is sufficiently smooth and non-zero then the asymptotic of Toeplitz determinant is given by Strong Szegö Theorem which states that

$$D_n[f] \sim E[f]G[f]^n \qquad n \to \infty \tag{C.3}$$

where functionals $E[f]$ and $G[f]$ are given by

$$G[f] = exp\ \hat{f}^0, \qquad E[f] = exp\sum_{k=1}^{\infty} k\hat{f}_k\hat{f}_{-k} \tag{C.4}$$

Here $\hat{f}_k$ are the Fourier coefficient of the expansion of the logarithm of $f(k)$

$$log\ f(q) \;=\; \sum_{k=-\infty}^{\infty}\hat{f}_k e^{ikq} \tag{C.5}$$

When the generating function has pointwise singularities or zeros then we can use Fisher-Hartwig Conjecture. When $f(q)$ has N singularities ar $q = \theta_i$ where $r = 1 \ldots N$ then

$$f(q) \;=\; g(q)\prod_{r=1}^{N} e^{i\kappa_r[(q-\theta_r)mod\ 2\pi-\pi]}(2-2cos(q-\theta_r))^{\lambda_r} \tag{C.6}$$

or equivalently after changing the variables $z = e^{iq}$

$$f(z) = g(z) \prod_{r=1}^{N} \left(1 - \frac{z}{z_r}\right)^{\kappa_r + \lambda_r} \left(1 - \frac{z_r}{z}\right)^{-\kappa_r + \lambda_r} \tag{C.7}$$

where $z_r = e^{i\theta_r}$. $g(q)$ is a smooth non-zero function with zero winding number. Then the asympthotic of Toeplitz determinant is given by

$$D_n[f] \;=\; E[g, \{\kappa_r\}, \{\lambda_r\}, \{\theta_r\}] n^{\sum_r (\lambda_r^2 - \kappa_r^2)} G[g]^n \qquad , n \to \infty \tag{C.8}$$

where

$$\begin{aligned} E[g, \{\kappa_r\}, \{\lambda_r\}, \{\theta_r\}] = \quad & E[g] \prod_{r=1}^{N} g_- \left(e^{i\theta_r}\right)^{-\kappa_r - \lambda_r} g_+ \left(e^{-i\theta_r}\right)^{\kappa_r - \lambda_r} \\ & \prod_{1 \le r \ne s \le N} (1 - e^{i(\theta_r - \theta_s)})^{(\kappa_r + \lambda_r)(\kappa_s - \lambda_s)} \\ & \prod_{r=1}^{N} \frac{G(1 + \kappa_r + \lambda_r) G(1 - \kappa_r + \lambda_r)}{G(1 + 2\lambda_r)} \end{aligned} \tag{C.9}$$

$G[g]$ and $E[g]$ are given by (C.4) and functions $g_\pm$ are given by a decomposition

$$g(q) \;=\; g_-(e_{iq}) G[g] g_+(e^{-iq}) \tag{C.10}$$

where g_+ and g_- are analytic and non-zero respectively inside and outside the unity circle on which g is defined and satisfy boundary conditions $g_+(0) = g_-(\infty) = 1$. G is Barnes G-function. This conjugare is proven for instence for $N = 1$.

If there exists inequivalent representetions of (C.6) asymphotic of Toeplitz determinant is given by generalized Fisher-Hadwig Conjecture. We label diffeerent parametrizations by index i and the conjugate says

$$D_n[f] \;=\; \sum_{i \in \Phi} E[g^i, \{\kappa_r^i\}, \{\lambda_r^i\}, \{\theta_r\}] n^{\Omega(i)} G[g^i]^n \qquad , n \to \infty \tag{C.11}$$

where

$$\Omega(i) = \sum_r ((\lambda_r^i)^2 - (\kappa_r^i)^2) \tag{C.12}$$

$$\Phi = \left\{ i : Re(\Omega(i)) = \max_j Re(\Omega(j)) \right\} \tag{C.13}$$

Publications

[I] L. Cincio, J. Dziarmaga, M.M. Rams, W.H. Zurek, "Entropy of entanglement and correlations induced by a quench: Dynamics of a quantum phase transition in the quantum Ising model", *Phys. Rev. A*, vol. 75, p. 052321, 2007.

[II] L. Cincio, J. Dziarmaga, J. Meisner , M.M. Rams, "Dynamics of a quantum phase transition with decoherence: Quantum Ising chain in a static spin environment", *Phys. Rev. B*, vol. 79, p. 094421 ,2009.

[III] J. Dziarmaga, M.M. Rams, "Dynamics of an inhomogeneous quantum phase transition", *New J. Phys*, vol. 12, p. 055007, 2010.

[IV] J. Dziarmaga, M.M. Rams, "Adiabatic dynamics of an inhomogeneous quantum phase transition: the case of a z>1 dynamical exponent", *New J. Phys.* vol. 12, p. 103002, 2010.

[V] L. Cincio, J. Dziarmaga, M.M. Rams, "Multiscale Entanglement Renormalization Ansatz in Two Dimensions: Quantum Ising Model", *Phys. Rev. Lett.*, vol. 75, p. 052321, 2008.

[VI] A. Niederberger, M.M. Rams, J. Dziarmaga, F.M. Cucchietti, J. Wehr, M. Lewenstein, "Disorder-induced order in quantum XY chain", *Phys. Rev. A* , vol. 82 , p. 013630, 2010.

[VII] M.M. Rams, B. Damski, "Quantum fidelity in the thermodynamic limit", ArXiv:1010.1048, 2010.

Bibliography

[1] J. A. Hertz, "Quantum critical phenomena," *Phys. Rev. B*, vol. 14, p. 1165, 1976.

[2] S. Sachdev, *Quantum Phase Transitions*. Cambridge, U.K.: Cambridge University Press, 1999.

[3] M. Greiner, O. Mandel, T. Esslinger, T. W. Hänsch, and I. Bloch, "Quantum phase transition from a superfluid to a mott insulator in a gas of ultracold atoms," *Nature*, vol. 415, pp. 39–44, Jan. 2002.

[4] R. Jördens, N. Strohmaier, K. Günter, H. Moritz, and T. Esslinger, "A Mott insulator of fermionic atoms in an optical lattice," *Nature*, vol. 455, pp. 204–207, Sept. 2008.

[5] R. Coldea, D. A. Tennant, E. M. Wheeler, E. Wawrzynska, D. Prabhakaran, M. Telling, K. Habicht, P. Smeibidl, and K. Kiefer, "Quantum criticality in an ising chain: Experimental evidence for emergent e_8 symmetry," *Science*, vol. 327, p. 177, 2010.

[6] L. E. Sadler, J. M. Higbie, S. R. Leslie, M. Vengalattore, and D. M. Stamper-Kurn, "Spontaneous symmetry breaking in a quenched ferromagnetic spinor bose-einstein condensate," *Nature*, vol. 443, p. 312, 2006.

[7] P. A. Lee, N. Nagaosa, and X.-G. Wen, "Doping a mott insulator: Physics of high-temperature superconductivity," *Rev. Mod. Phys.*, vol. 78, pp. 17–85, Jan 2006.

[8] T. W. B. Kibble, "Topology of cosmic domains and strings," *Journal of Physics A Mathematical General*, vol. 9, pp. 1387–1398, Aug. 1976.

[9] W. H. Zurek, "Cosmological experiments in superfluid helium?," *Nature*, vol. 317, pp. 505–508, Oct. 1985.

[10] P. Laguna and W. H. Zurek, "Density of kinks after a quench: When symmetry breaks, how big are the pieces?," *Phys. Rev. Lett.*, vol. 78, pp. 2519–2522, Mar 1997.

[11] G. J. Stephens, L. M. A. Bettencourt, and W. H. Zurek, "Critical dynamics of gauge systems: Spontaneous vortex formation in 2d superconductors," *Phys. Rev. Lett.*, vol. 88, p. 137004, Mar 2002.

[12] I. Chuang, B. Yurke, R. Durrer, and N. Turok, "Cosmology in the laboratory - Defect dynamics in liquid crystals," *Science*, vol. 251, pp. 1336–1342, Mar. 1991.

[13] M. J. Bowick, L. Chandar, E. A. Schiff, and A. M. Srivastava, "The Cosmological Kibble Mechanism in the Laboratory: String Formation in Liquid Crystals," *Science*, vol. 263, pp. 943–945, Feb. 1994.

[14] C. Bäuerle, Y. M. Bunkov, S. N. Fisher, H. Godfrin, and G. R. Pickett, "Laboratory simulation of cosmic string formation in the early Universe using superfluid ^{3}He," *Nature*, vol. 382, pp. 332–334, July 1996.

[15] V. M. H. Ruutu, V. B. Eltsov, A. J. Gill, T. W. B. Kibble, M. Krusius, Y. G. Makhlin, B. Plaçais, G. E. Volovik, and W. Xu, "Vortex formation in neutron-irradiated superfluid ^{3}He as an analogue of cosmological defect formation," *Nature*, vol. 382, pp. 334–336, July 1996.

[16] A. Maniv, E. Polturak, and G. Koren, "Observation of magnetic flux generated spontaneously during a rapid quench of superconducting films," *Phys. Rev. Lett.*, vol. 91, p. 197001, Nov 2003.

[17] R. Monaco, J. Mygind, M. Aaroe, R. J. Rivers, and V. P. Koshelets, "Zurek-kibble mechanism for the spontaneous vortex formation in $nb-al/al_{ox}/nb$ josephson tunnel junctions: New theory and experiment," *Phys. Rev. Lett.*, vol. 96, p. 180604, May 2006.

[18] S. Ducci, P. L. Ramazza, W. González-Viñas, and F. T. Arecchi, "Order parameter fragmentation after a symmetry-breaking transition," *Phys. Rev. Lett.*, vol. 83, pp. 5210–5213, Dec 1999.

[19] S. Casado, W. González-Viñas, S. Boccaletti, P. L. Ramazza, and H. Mancini, "The birth of defects in pattern formation: Testing of the Kibble Zurek mechanism," *European Physical Journal Special Topics*, vol. 146, pp. 87–98, July 2007.

[20] D. R. Scherer, C. N. Weiler, T. W. Neely, and B. P. Anderson, "Vortex formation by merging of multiple trapped bose-einstein condensates," *Phys. Rev. Lett.*, vol. 98, p. 110402, Mar 2007.

[21] J. Dziarmaga, A. Smerzi, W. H. Zurek, and A. R. Bishop, "Dynamics of quantum phase transition in an array of josephson junctions," *Phys. Rev. Lett.*, vol. 88, p. 167001, Apr 2002.

[22] W. H. Zurek, U. Dorner, and P. Zoller, "Dynamics of a Quantum Phase Transition," *Phys. Rev. Lett.*, vol. 95, p. 105701, Sept. 2005.

[23] J. Dziarmaga, "Dynamics of a quantum phase transition and relaxation to a steady state," *Advances in Physics*, vol. 59, pp. 1063–1189, Nov. 2010.

[24] A. Polkovnikov, K. Sengupta, A. Silva, and M. Vengalattore, "Nonequilibrium dynamics of closed interacting quantum systems," *ArXiv e-prints*, July 2010.

[25] R. P. Feynman, "Simulating Physics with Computers," *International Journal of Theoretical Physics*, vol. 21, pp. 467–488, June 1982.

[26] S. Lloyd, "Universal Quantum Simulators," *Science*, vol. 273, pp. 1073–1078, Aug. 1996.

[27] D. Aharonov, W. van Dam, J. Kempe, Z. Landau, S. Lloyd, and O. Regev, "Adiabatic Quantum Computation is Equivalent to Standard Quantum Computation," *ArXiv Quantum Physics e-prints*, May 2004.

[28] M. Lewenstein, A. Sanpera, V. Ahufinger, B. Damski, A. Sen, and U. Sen, "Ultracold atomic gases in optical lattices: mimicking condensed matter physics and beyond," *Advances in Physics*, vol. 56, p. 243, 2007.

[29] J. Dziarmaga, "Dynamics of a Quantum Phase Transition: Exact Solution of the Quantum Ising Model," *Phys. Rev. Lett.*, vol. 95, p. 245701, Dec. 2005.

[30] B. Damski, "The simplest quantum model supporting the kibble-zurek mechanism of topological defect production: Landau-zener transitions from a new perspective," *Phys. Rev. Lett.*, vol. 95, p. 035701, Jul 2005.

[31] B. Damski and W. H. Zurek, "Adiabatic-impulse approximation for avoided level crossings: From phase-transition dynamics to landau-zener evolutions and back again," *Phys. Rev. A*, vol. 73, p. 063405, Jun 2006.

[32] A. Polkovnikov, "Universal adiabatic dynamics in the vicinity of a quantum critical point," *Phys. Rev. B*, vol. 72, pp. 161201–+, Oct. 2005.

[33] L.D. Landau and E.M. Lifshitz, *Quantum Mechanics*, Pergamon, 1958; C. Zener, Proc. Roy. Soc. Lond. A **137**, 696 (1932).

[34] R. W. Cherng and L. S. Levitov, "Entropy and correlation functions of a driven quantum spin chain," *Phys. Rev. A*, vol. 73, p. 043614, Apr 2006.

[35] M. A. Nielsen and I. L. Chuang, *Quantum Computation and Quantum Information*. Cambridge University Press, 2000.

[36] P. Zanardi and N. Paunković, "Ground state overlap and quantum phase transitions," *Phys. Rev. E*, vol. 74, p. 031123, Sep 2006.

[37] C. de Grandi, V. Gritsev, and A. Polkovnikov, "Quench dynamics near a quantum critical point," *Phys. Rev. B*, vol. 81, pp. 012303–+, Jan. 2010.

[38] S. Fölling, A. Widera, T. Müller, F. Gerbier, and I. Bloch, "Formation of spatial shell structure in the superfluid to mott insulator transition," *Phys. Rev. Lett.*, vol. 97, p. 060403, Aug 2006.

[39] G. K. Campbell, J. Mun, M. Boyd, P. Medley, A. E. Leanhardt, L. G. Marcassa, D. E. Pritchard, and W. Ketterle, "Imaging the Mott Insulator Shells by Using Atomic Clock Shifts," *Science*, vol. 313, pp. 649–652, Aug. 2006.

[40] T. W. B. Kibble and G. E. Volovik, "On phase ordering behind the propagating front of a second-order transition," *ZhETF Pis ma Redaktsiiu*, vol. 65, pp. 96–+, Jan. 1997.

[41] J. Dziarmaga, P. Laguna, and W. H. Zurek, "Symmetry breaking with a slant: Topological defects after an inhomogeneous quench," *Phys. Rev. Lett.*, vol. 82, pp. 4749–4752, Jun 1999.

[42] N. B. Kopnin and E. V. Thuneberg, "Time-dependent ginzburg–landau analysis of inhomogeneous normal-superfluid transitions," *Phys. Rev. Lett.*, vol. 83, pp. 116–119, Jul 1999.

[43] E. H. Lieb and D. W. Robinson, "The finite group velocity of quantum spin systems," *Communications in Mathematical Physics*, vol. 28, pp. 251–257, Sept. 1972.

[44] T. Platini, D. Karevski, and L. Turban, "Gradient critical phenomena in the Ising quantum chain," *Journal of Physics A Mathematical General*, vol. 40, pp. 1467–1479, Feb. 2007.

[45] W. H. Zurek and U. Dorner, "Phase transition in space: how far does a symmetry bend before it breaks?," *Royal Society of London Philosophical Transactions Series A*, vol. 366, pp. 2953–2972, Aug. 2008.

[46] B. Damski and W. H. Zurek, "How to fix a broken symmetry: quantum dynamics of symmetry restoration in a ferromagnetic Bose Einstein condensate," *New Journal of Physics*, vol. 10, pp. 045023–+, Apr. 2008.

[47] S. Deng, G. Ortiz, and L. Viola, "Anomalous nonergodic scaling in adiabatic multicritical quantum quenches," *Phys. Rev. B*, vol. 80, p. 241109, Dec 2009.

[48] S. Mostame, G. Schaller, and R. Schützhold, "Decoherence in a dynamical quantum phase transition of the transverse ising chain," *Phys. Rev. A*, vol. 76, p. 030304, Sep 2007.

[49] A. Fubini, G. Falci, and A. Osterloh, "Robustness of adiabatic passage through a quantum phase transition," *New Journal of Physics*, vol. 9, pp. 134–+, May 2007.

[50] D. Patanè, A. Silva, L. Amico, R. Fazio, and G. E. Santoro, "Adiabatic dynamics in open quantum critical many-body systems," *Phys. Rev. Lett.*, vol. 101, p. 175701, Oct 2008.

[51] D. S. Fisher, "Critical behavior of random transverse-field ising spin chains," *Phys. Rev. B*, vol. 51, pp. 6411–6461, Mar 1995.

[52] J. Dziarmaga, "Dynamics of a quantum phase transition in the random ising model: Logarithmic dependence of the defect density on the transition rate," *Phys. Rev. B*, vol. 74, p. 064416, Aug 2006.

[53] T. Caneva, R. Fazio, and G. E. Santoro, "Adiabatic quantum dynamics of a random Ising chain across its quantum critical point," *Rhys. Rev. B*, vol. 76, pp. 144427–+, Oct. 2007.

[54] J. E. Bunder and R. H. McKenzie, "Effect of disorder on quantum phase transitions in anisotropic XY spin chains in a transverse field," *Phys. Rev. B*, vol. 60, pp. 344–358, July 1999.

[55] P. Jordan and E. Wigner, "Über das Paulische Äquivalenzverbot," *Zeitschrift fur Physik*, vol. 47, pp. 631–651, Sept. 1928.

[56] T. Ehrhardt and S. B., "Toeplitz determinants with one fisherÐhartwig singularity," *Journal of Functional Analysis*, vol. 148, pp. 229–256, 1997.